AEROTHERM FINAL REPORT 77-239

(NASA-CR-150271)   BOUNDARY LAYER INTEGRAL   N77-24189
MATRIX PROCEDURE: VERIFICATION OF MODELS
Final Report (Aerotherm Corp.)   74 p
HC A04/MF A01   CSCL 21H   Unclas
                                                    G3/20 · 29133

Aerotherm Project 7239

April 1977

BOUNDARY LAYER INTEGRAL MATRIX
# PROCEDURE: VERIFICATION OF MODELS

By William S. Bonnett and R. Michael Evans

Distribution of this report is provided in the interest
of information exchange. Responsibility for the contents
resides in the author or organization that prepared it.

JUN 1977
RECEIVED
NASA STI FACILITY:
INPUT BRANCH

Prepared under Contract No. NAS8-31961
ACUREX CORPORATION/AEROTHERM DIVISION
485 Clyde Avenue
Mountain View, California   94042

for

NATIONAL AERONAUTICS AND SPACE ADMINISTRATION
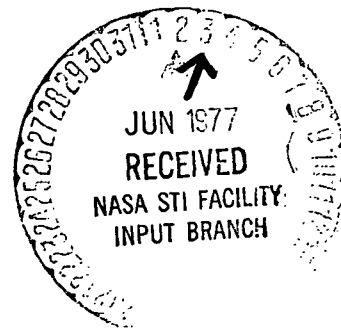
Page
Intentionally
Left Blank

ABSTRACT

A study of the three turbulent models (Kendall, Cebeci-Smith, and Bushnell-Beckwith) currently available in the JANNAF version of the Aerotherm Boundary Layer Integral Matrix Procedure (BLIMP-J) code is presented in this report. (The BLIMP-J program is the standard prediction method for boundary layer effects in liquid rocket engine thrust chambers.) Experimental data from flow fields with large edge-to-wall temperature ratios ($T_e/T_w > 5$) are compared to the predictions of the three turbulence models contained in BLIMP-J. In addition, test conditions necessary to generate additional data on a flat plate or in a nozzle are given. This study concludes that the Cebeci-Smith turbulence model be the recommended model for the prediction of boundary layer effects in liquid rocket engines.

In addition, a brief study of the effects of homogeneous chemical reaction kinetics for a hydrogen/oxygen system shows that for most flows, kinetics are probably only significant for stoichiometric mixture ratios.

Page
Intentionally
Left Blank

TABLE OF CONTENTS

LIST OF ILLUSTRATIONS

SECTION 1

INTRODUCTION AND SUMMARY

Accurate predictions of the thrust loss caused by boundary layer effects and of the heat flux to the wall are required for proper design and performance evaluation of rocket nozzles. This work is part of a continuing effort to upgrade predictive techniques for liquid propellant rocket motors in order to provide the best computational tools available for the series of JANNAF programs.

Three turbulence models (Kendall, Cebeci-Smith, and Bushnell-Beckwith (Reference 1)) can be used with the BLIMP-J code to predict boundary layer effects. In liquid propellant rocket motors, the boundary layers are usually both turbulent and highly cooled by the nozzle walls. This report presents the results of a study to determine the most suitable turbulence model for predicting boundary layer effects under these conditions. Also presented are assessments of the impact of transport properties (viscosity, conductivity, diffusion coefficients) and the impact of equilibrium properties on thrust loss and heat flux calculations. In addition, procedures for handling nonideal flows are described.

Results indicate that the Cebeci-Smith model gives the best agreement with available data, and this model is therefore recommended as the standard turbulence model. In addition, we found that turbulent boundary layer predictions are insensitive to reasonable variations (±20 percent) in the transport properties, and the ideal gas law is adequate for most nozzle performance predictions. Chemical reaction kinetics appeared to be unimportant, except near stoichiometric conditions (MR = 8), for hydrogen/oxygen systems and flow conditions appropriate to the Space Shuttle Main Engine (SSME).

The technical program was divided into four major tasks:

- Turbulent model recommendation and models sensitivity investigation

- Recommendation of Test Program

- Investigation of the importance of gas phase kinetics

- Suggestions for improvements to BLIMP-J and miscellaneous code modifications

Each of these tasks is described in the following sections of this report. Conclusions and recommendations resulting from these tasks are given in Section 6. In addition, one appendix (Appendix C) is included under separate cover. This appendix contains corrections and modified pages for the BLIMP-J User's Manual.

SECTION 2

TURBULENCE MODEL RECOMMENDATION

The objective of this task was to identify which of the three turbulence models available in BLIMP-J produced analytical predictions in acceptable agreement with existing test data for highly cooled walls. Analytical predictions with a constant set of program input data have indicated that the turbulence models calculate significantly different heat fluxes and thrust decrements for flow conditions where the boundary layer edge-to-wall temperature ratio is greater than five. In these cases large property variations occur in the near wall region. Two of the models (Kendall and Cebeci-Smith) use the same formulation in the wake region, but differ significantly in the "law of the wall" region. Since the condition of large property variation near the wall exists in liquid rocket engines, it is particularly important to determine which of the models best describes this type of flow.

In order to accomplish this objective, the task was divided into three subtasks: the data search, analytical solutions and comparisons with data, and a short sensitivity study. These subtasks are described in the following subsections.

2.1   DATA SEARCH

A survey was conducted to locate adequate test data from shock tube experiments, combustion flow tests, or tests with large edge-to-wall temperature ratios. There were three objectives to be accomplished in this subtask:

●   Identify essential requirements and range of the data for important flow parameters

●   Identify and contact data sources

●   Determine if the data could be used to select the most appropriate turbulence model for use in the prediction methodology

3

To be considered, the flow had to be fully turbulent ($Re_x \sim 10^6$) and have large edge-to-wall static temperature ratio (>5). For airflows, these conditions can be satisfied by a flow with:

$P_0 \sim 1.013 \times 10^6$ N/m^2 (10 atm)

$T_0 \sim 1,800°$K   (3,240°R)

$T_w \sim 300°$K   (540°R)

A few feet of running length and expansion to approximately Mach 1 provides unit Reynolds numbers up to 500×10^6. Data similar to that of Back & Cuffel (Reference 2, used for previous BLIMP verification) would have been ideal if the stagnation temperature (850°K) was considerably higher (~1,800°K) or the wall temperature (>383°K) was slightly lower (~300°K)

In addition, sufficient detail in the data was needed to allow comparisons with BLIMP to be made. The minimum information needed for a BLIMP prediction is:

- Flow geometry and gas composition

- Stagnation pressure and temperature

- Wall temperature distribution

- Edge pressure distribution

Data useful for comparison of predictions with experiment include:

- Wall heat flux distribution

- Velocity (or Mach Number) profiles

- Temperature profiles

- Wall shear measurements

However, not all of this data was required for comparison. For example, heat flux measurements were sufficient for most comparisons.

It was also desirable to know where and how the flow became turbulent. Data near the transition point or in the transition region can be misleading with respect to turbulent model verification. The best way to start the predictions is with initial conditions that use experimental velocity and temperature profiles in the fully turbulent region. However, flows with very short transition lengths and well-defined turbulent starting locations are acceptable.

4

The types of flow considered were:

- Subsonic and supersonic internal air flows similar to that of Back & Cuffel (Reference 2)

- Shock tube flows

- Combustion gas flows, including liquid rocket motor tests, with very high stagnation temperatures

- Arc heater and high-speed wind tunnel flows over blunt bodies

The laboratory air flows were the most suitable, since they are usually well defined and provide sufficient data. Shock tube flows satisfy the temperature ratio criteria, but introduce the problems of transient behavior, dissociation of gas, and possible chemical kinetic effects in the boundary layer. Combustion flows have problems of incomplete mixing or striated core flows and scattered data. External flows in reentry tests are subject to entropy swallowing and transition effects, which may invalidate the models or the prediction method.

The agencies and individuals contacted in the data search are listed in Table 1. In most cases, these sources did not have suitable data nor did they know any appropriate data. However, several agencies provided assistance, as discussed below:

- NASA-Huntsville — Klaus Gross supplied data on the 40K model SSME tests and predictions for the RL-10 engine tests

- JPL — Although he could not help with locating data, Lloyd Back suggested that the desired data can be obtained with the experimental facility at JPL

- NASA-Lewis — Don Boldman suggested that we contact a professor at the University of Berlin who had catalogued for reference an extensive amount of data, and who might be able to assist in the data search. A letter was mailed to Germany; however, no reply was ever received

- Rocketdyne — The wall heat flux measurements taken from hot fired tests of a 3K SSME model engine were made available

TABLE 1.   AGENCIES CONTACTED DURING DATA SEARCH

Arnold Engineering & Development Center (AEDC)

Avco-Everett (Robert Kessler)

Fluidyne (Owen Lamb)

Jet Propulsion Lab (Lloyd Back, Ray Kushida)

McDonnell-Douglas (Tuncer Cebeci, Calvin Kaupts)

NASA-Ames

NASA-Huntsville (Klaus Gross)

NASA-Langley

NASA-Lewis (Don Boldman)

Naval Ordance Lab (NOL)

Ohio State (Robert Nerem)

Rocketdyne (George Osugi)

Stanford University

TRW (Wally Geniec)

University of California, Berkeley

UTC

● Ohio State — Professor Robert Nerem provided additional information on heat transfer measurements in a shock tube experiment reported in References 3 and 4

The data search uncovered very few experimental studies of highly cooled turbulent boundary layers with the desired temperature ratio and no single study with appropriate flow conditions. The data search showed that with the exception of hot-fired motor tests and shock tubes, data with edge-to-wall temperature ratios greater than five were not available.

2.2 ANALYTICAL SOLUTIONS

The first data analyzed were from an experimental shock tube investigation of heat transfer to a cylinder with a sharp leading edge (Reference 3). A schematic of the apparatus is given in Figure 1 and the flow conditions are given in Table 2. The driver gas was helium, and the driven gas was air. The Reynolds number was on the order of 3×10^7/meter, and the edge-to-wall temperature ratio ranged between 10 and 23. The flow was artificially tripped; however, most of the data is far enough downstream of the trip so that low Reynolds number overshoot is not a significant factor.*

---

*An abnormally large increase in wall shear and wall heat flux has been observed for low Reynolds number flows in the region just downstream of a boundary layer trip. This "low Reynolds number amplification" has been attributed to the transitional structure of the flow and is a function of the relative proximity to the trip (transition point). For the three cases studied here, the first heat flux measurements were at $\delta* = 4100$, 6970 and 6250. The variable $\delta*$ is a normalized boundary layer thickness defined by:

$$\delta* = \frac{\delta_{98}\rho_w}{\mu_w} \sqrt{\frac{\tau_w}{\rho_w} g_c}$$

where δ_{98} is the distance normal to the wall at which $u/u_e = 0.98$, τ_w is the shear stress at the wall, ρ_w is the density at the wall, and μ_w is the viscosity at the wall. For values of $\delta*$ greater than 2000, low Reynolds number overshoot is not important. Therefore, the heat flux measurements are sufficiently far downstream of the trip so that the flow is fully turbulent.
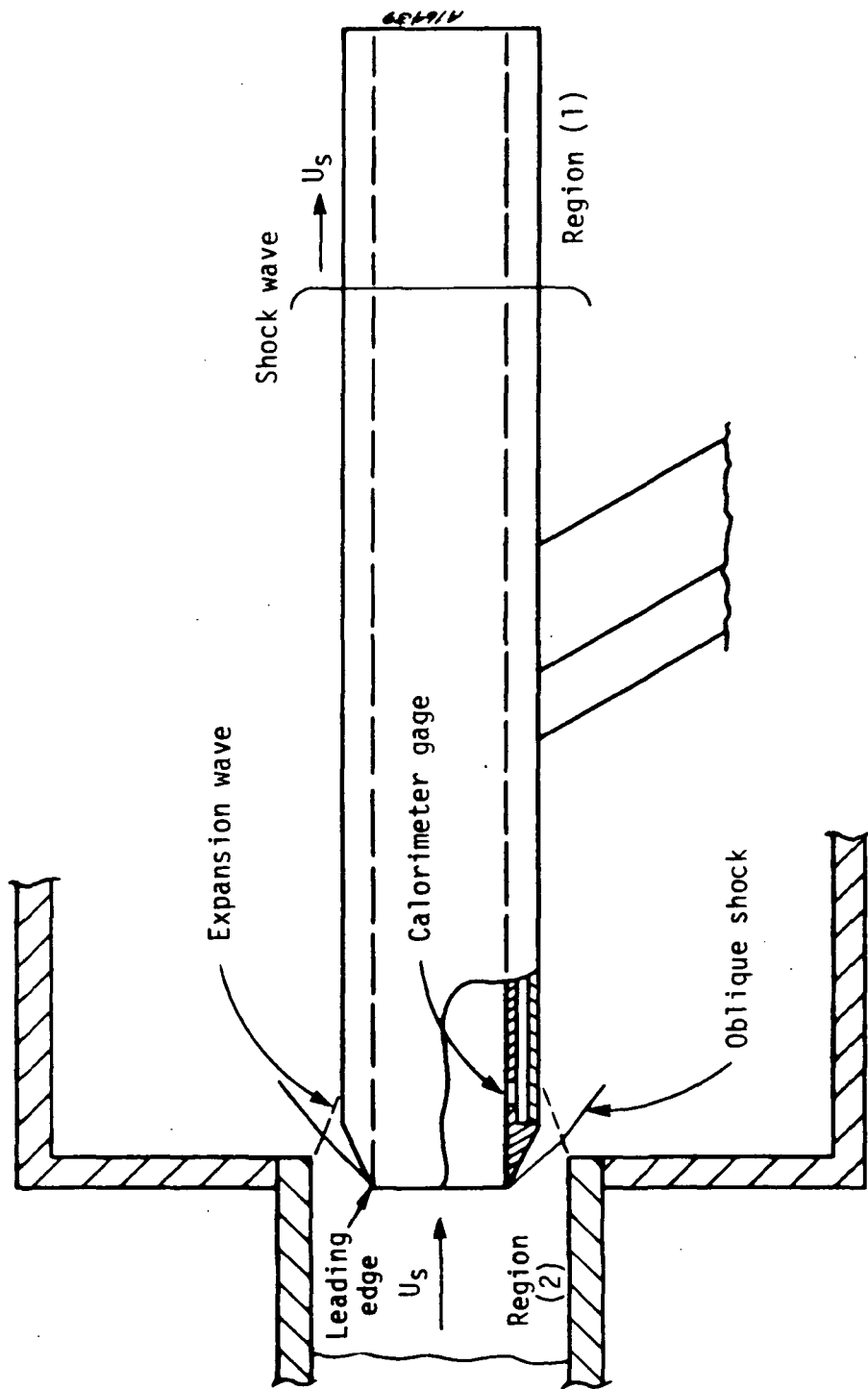
Figure 1. Hollow cylinder heat transfer model (Hopkins (Reference 4)).

8

TABLE 2. FLOW CONDITIONS IN SHOCK TUBE

P_{stag}	u_2, P_2,	⟵ u_s	P_1
H_{stag}	T_2		T_1

Region 1:   Upstream of shock wave

Region 2:   Downstream of shock wave

Stagnation Region: Stagnation conditions for Region 2 flow

Nerem Case A

P_1 = 0.002665 MN/m² (20 mm Hg)	P_2 = 0.3705 MN/m²	P_{stag} = 8.8162 MN/m²
u_s = 3650 m/sec (3.65 mm/μsec)	u_2 = 3267.5 m/sec	u = 0
T_1 = 300°K	T_2 = 3960.3°K	T_{stag} = 6476.7°K
γ = 1.44	γ = 1.19	γ = 1.20
h_1 = 0.01662 MJ/kg	h_2 = 6.602 MJ/kg	h_{stag} = 11.94 MJ/kg

Re_x = 0.11 x 10⁶ to 0.999 x 10⁶, Re_θ = 509 to 3360

Nerem Case B

P_1 = 0.00133 MN/m² (10 mm Hg)	P_2 = 0.82987 MN/m²	P_{stag} = 12.50 MN/m²
u_s = 4850 m/sec (4.85 mm/μsec)	u_2 = 4392.8 m/sec	u = 0
T_1 = 300°K	T_2 = 5672.2°K	T_{stag} = 8590°K
γ = 1.44	γ = 1.18	γ = 1.19
h_1 = 0.0166 MJ/kg	h_2 = 11.688 MJ/kg	h_{stag} = 21.317 MJ/kg

Re_x = 0.15 x 10⁶ to 0.69 x 10⁶, Re_θ = 427 to 2394

Nerem Case C

P_1 = 0.001333 MN/m² (10 mm Hg)	P_2 = 0.22498 MN/m²	P_{stag} = 6.32552 MN/m²
u_s = 4010 m/sec (4.01 mm/μsec)	u_2 = 3616.8 m/sec	u = 0
T_1 = 300°K	T_2 = 4292°K	T_{stag} = 7115.6°K
γ = 1.44	γ = 1.22	γ = 1.19
h_0 = 0.0166 MJ/kg	h_2 = 7.976 MJ/kg	h_{stag} = 14.517 MJ/kg

Re_x = 0.061 x 10⁶ to 0.55 x 10⁶, Re_θ = 337 to 2100

The heat transfer to the inside of the cylinder was measured with thick film platinum calorimeters, approximately 25.4 μm thick (0.001 inch) mounted on Lucite substrates flush with the surface. The protrusion of the gauges into the flow induced transition from laminar to turbulent flow in the absence of a tripping element. For the runs investigated, a 178 μm (0.007 inch) tripping element was placed at 1.27 and 2.54 cm (0.5 and 1.0 inch) from the leading edge. The heat flux was measured at 2.54, 6.35, 8.89, 11.45, and 13.97 cm (1, 2.5, 3.5, 4.5, and 5.5 inches), although not all in the same runs. The wall temperature was 298°K (room temperature) in all cases.

Comparisons of the predictions of the three turbulent models and the data are shown in Figures 2, 3, and 4. The laminar prediction and data are in very good agreement (see Figure 3). Comparison of the turbulent results show that in all cases the heat flux predictions of the Kendall model are too high by a factor of approximately two. The best fit for this data is provided by either the Cebeci-Smith or Bushnell-Beckwith models, but in some cases values of Re_θ (600 to 1500) are below the optimum range for the Cebeci model.

Another shock tube experiment was also used for comparison. The experiments of Jones (Reference 4) show length Reynolds numbers that vary from 10^6 to 10^7 and values of T_e/T_w that vary from 5 to 14. The data lack the desired detail and are somewhat scattered, but have proved to be useful. The heat flux data were found to correlate fairly well (as shown in Figure 5) with the classical incompressible, flat plate results employing the modified Reynolds analogy,* represented by the equation:

$$St = 0.0296 \, Re_x^{-0.2} Pr^{-2/3} \tag{1}$$

where

$$St = \frac{\dot{q}}{\rho_e u_e (H_e - H_w)} \tag{2}$$

---

*It is interesting to note, however, that for the conditions of the Nerem and Hopkins experiments the correlations of Equation (1) did not fit the data, by a factor of about 2, and that the Kendall model was much closer to the correlation than the Cebeci model. Thus, agreement between the data and the correlation of Equation (1) may be fortuitous.
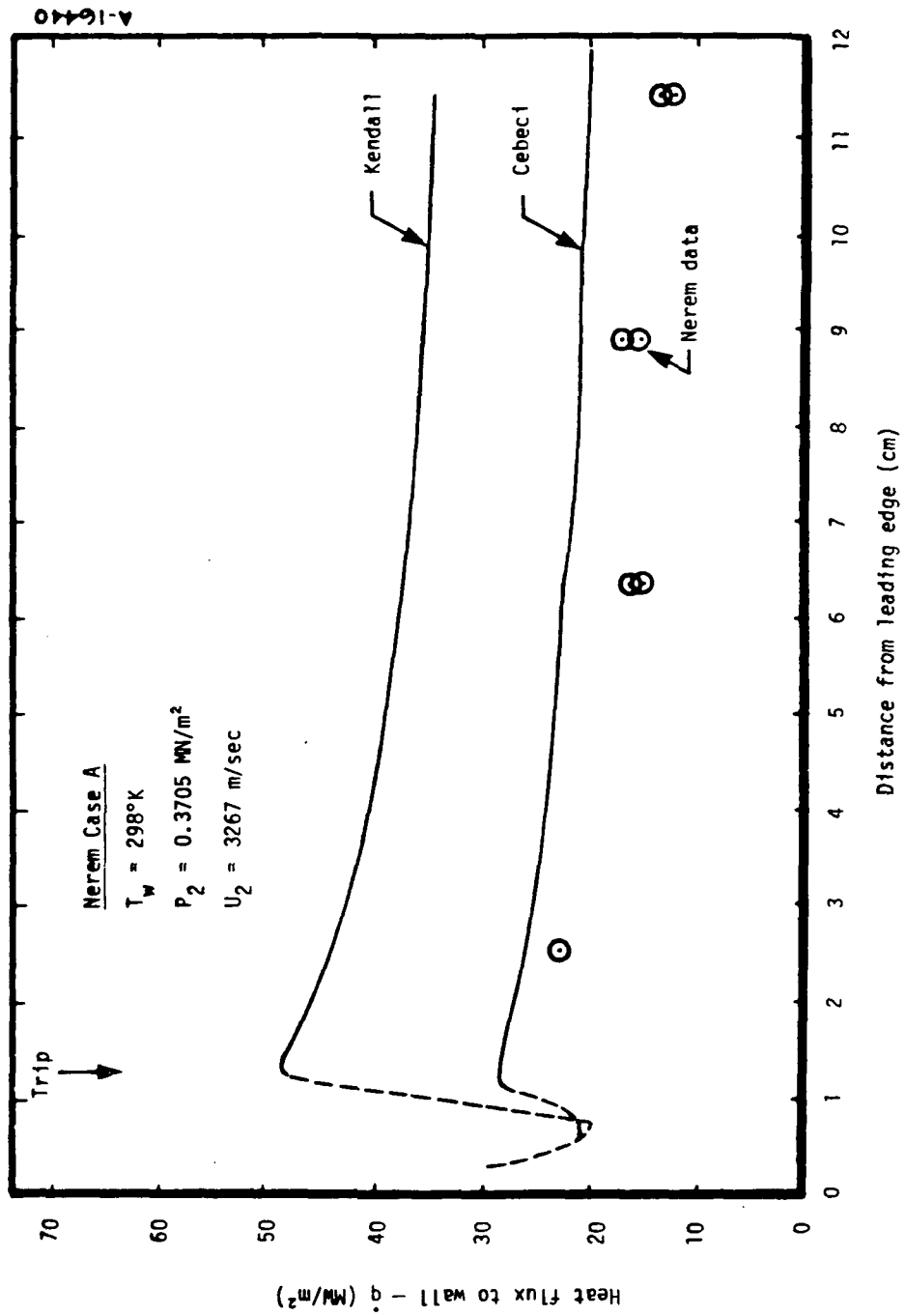
Figure 2. Axial heat flux distribution — Nerem Case A.

Nerem Case A

$T_w = 298°K$

$P_2 = 0.3705 \ MN/m^2$

$U_2 = 3267 \ m/sec$

Trip

Kendall

Cebeci

Nerem data

Heat flux to wall — $\dot{q}$ (MW/m^2)
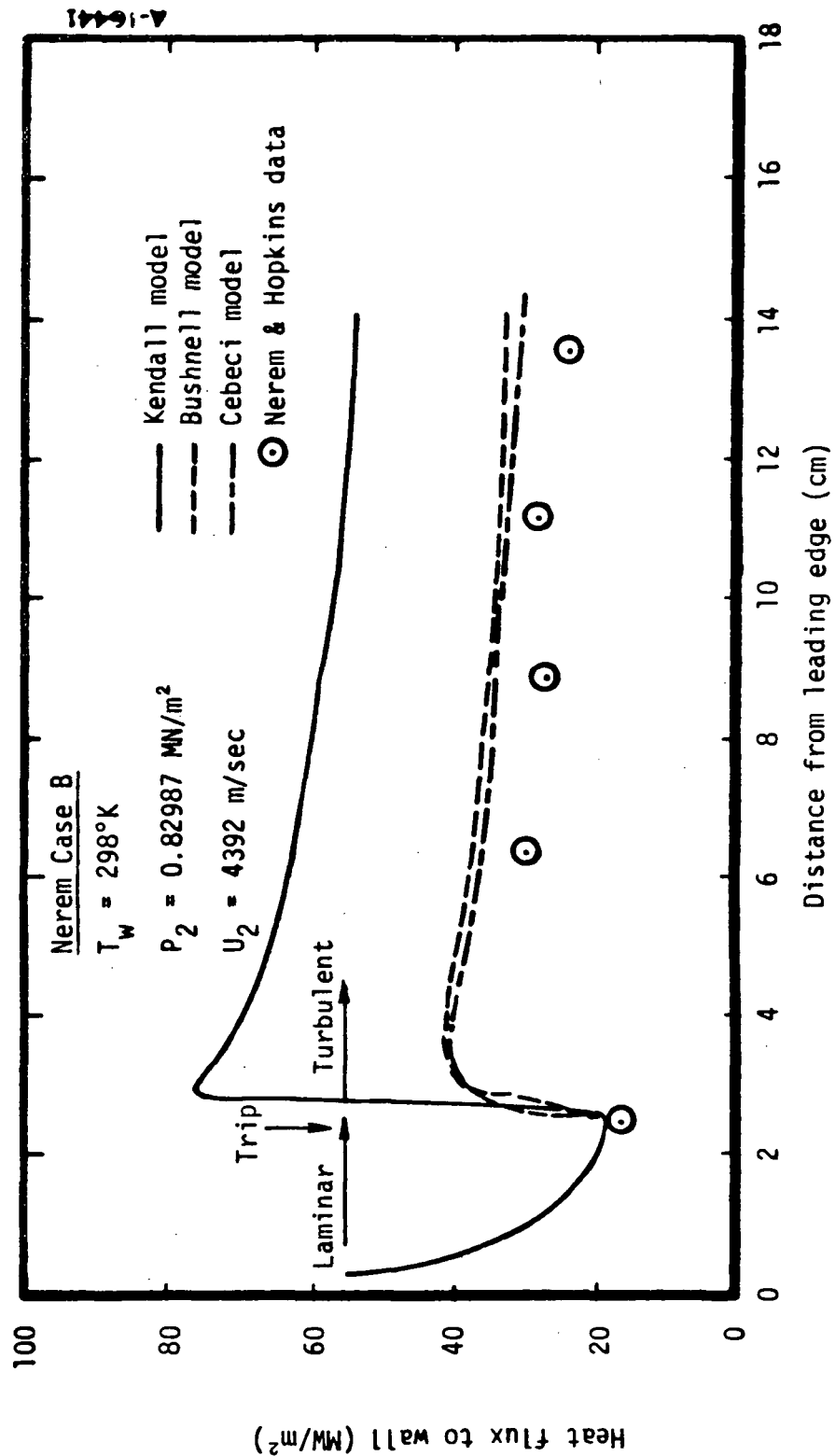
Distance from leading edge (cm)

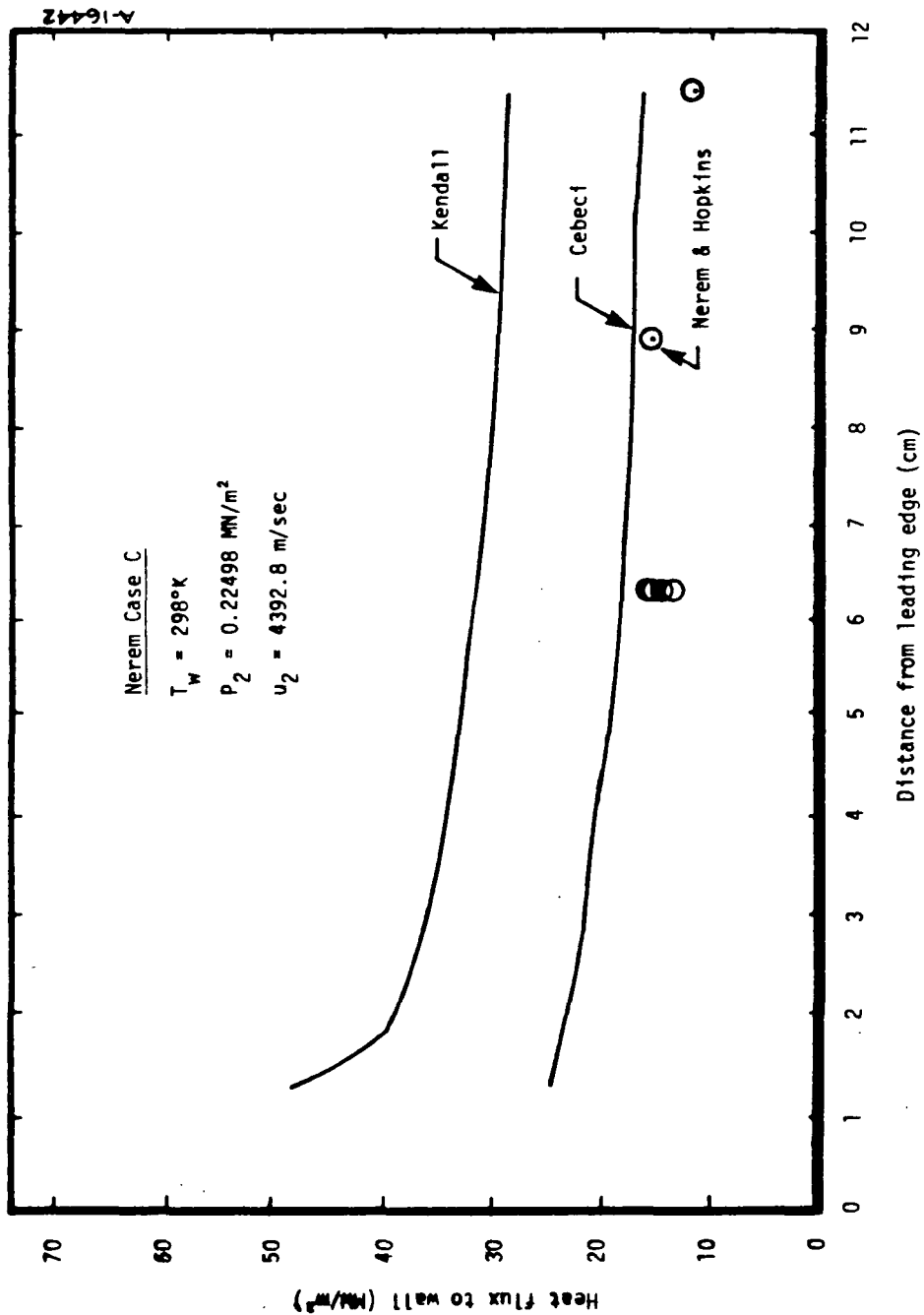Figure 3. Axial heat flux distribution — Nerem Case B.

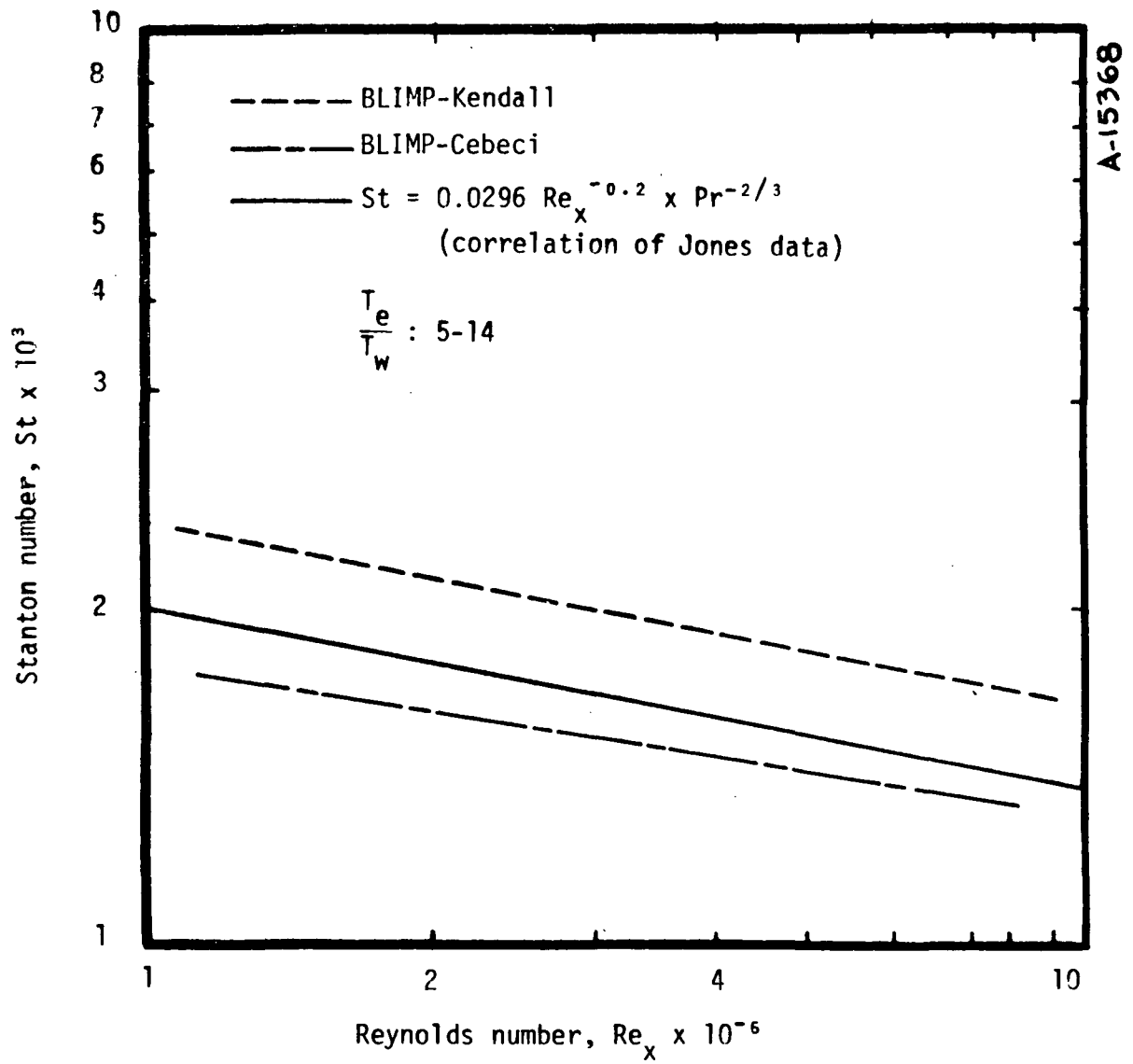Figure 4. Axial heat flux distribution — Nerem Case C.

13

Figure 5. BLIMP comparisons with correlation of Jones data (Reference 5).

14

and H_e is the total enthalpy of the freestream gas. In Equations (1) and
(2), all properties are evaluated at the freestream gas conditions.

The BLIMP program with the Kendall and Cebeci models was used to pre-
dict the heat flux for several of the flow conditions of the Jones experi-
ments. A comparison of these predictions and the correlation given in Equa-
tion (1) (with Pr = 0.7) is shown in Figure 5. The Cebeci model fits the
data better than the Kendall model.

Experimental data from the 3K SSME scaled model hot-fired tests were
used for comparison with the predictions of the models (Reference 9). The
regeneratively-cooled model could not provide chamber thermal conditions, so
a calorimetrically instrumented version was also fired. The data from the
calorimeter thrust chamber were used for our comparisons. The problem with
these data is that the mixture ratio near the wall is a critical but unknown
value. Due to uncertainties in the injector pattern, striations in the flow,
or bad mixing of oxidizer and fuel, it is possible to have a mixture ratio
(in some regions of the flow) which is much different than the nominal value.
This difference is always a problem with liquid rocket engine test data, and
is the reason why this type of data is not generally used for this type of
verification of predictive models. With the nominal mixture ratio of 5.443,
the experimental data indicate that the Cebeci model predicts heat transfer
most accurately, as is shown in Figure 6. If the mixture ratio used in the
predictions is reduced to 3, the Kendall model gives excellent agreement.
Unfortunately, it is not possible to rule out a mixture ratio of 3 near the
wall.

Data from several other hot-fired tests were also examined. In gen-
eral, the data consisted of the mixture ratio, chamber pressure and total
heat flux to the wall. Axial pressure profiles were obtained from the TDK
program, while wall temperature profiles were obtained either from calorim-
eter chamber tests of similar nozzles or from theoretical extensions (scale-
up) of calorimeter results. In all cases, the exact value of the mixture
ratio in the boundary layer is not known, which can cause significant uncer-
tainty in the predictions, as described above. Comparisons of the predic-
tions with the experimental measurements are summarized below.
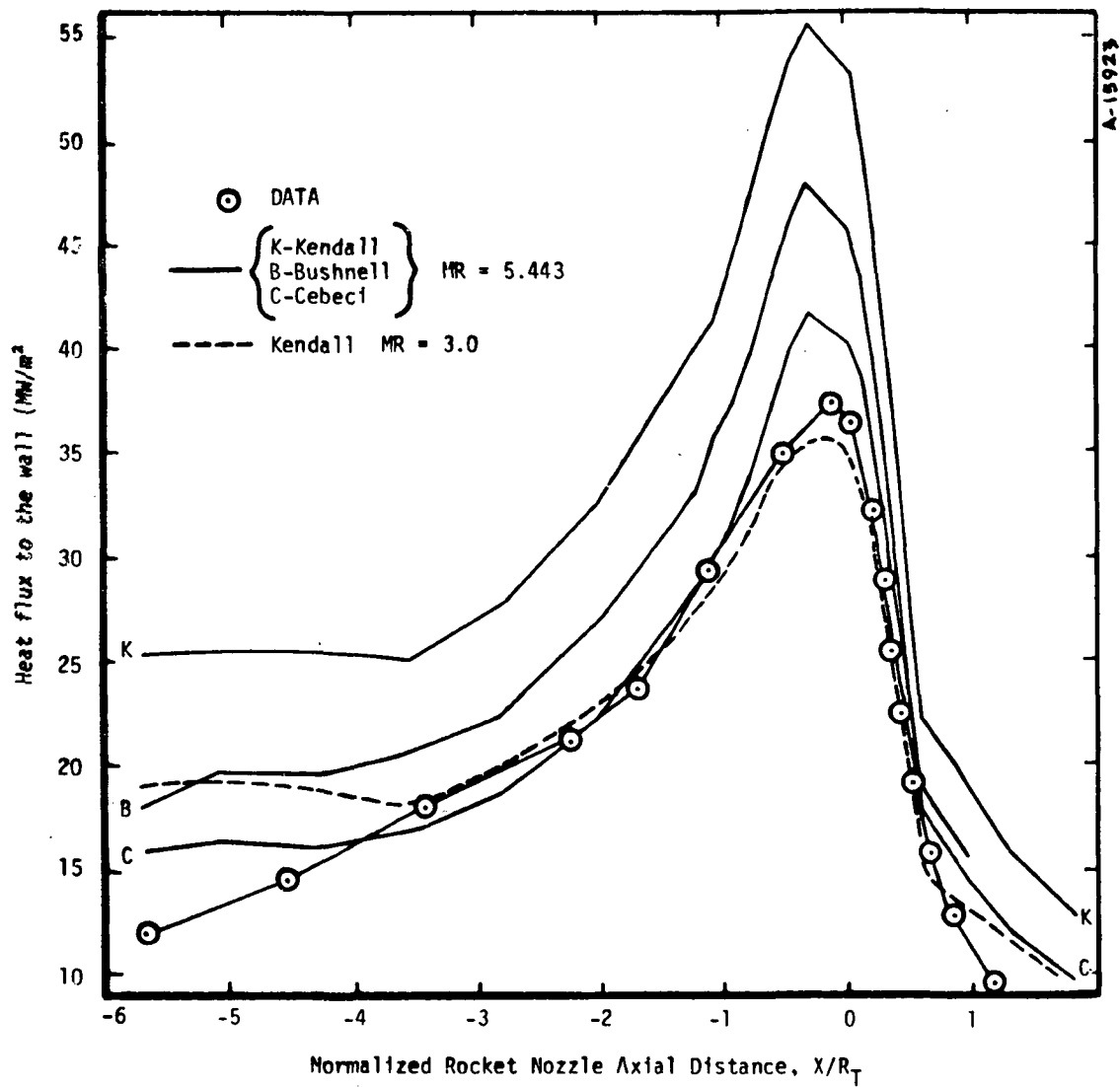
Figure 6. Heat flux prediction for 3K calorimeter chamber.

3K SSME Scaled Model, Regeneratively Cooled

For these tests, the total heat flux prediction of the Cebeci model was 5 percent higher than the measured value. This prediction gave the closest agreement with the measured values. The result from the Bushnell model was 20 percent higher than the measured value, and the Kendall model prediction was 60 percent higher. No attempt was made to investigate the effect of changing the mixture ratio.

40K SSME Scaled Model, Regeneratively Cooled

Here, the total heat flux to the walls was best predicted by the Kendall model. This model was 5 percent higher than the measured value. The Bushnell model prediction was 18 percent lower than the measured data, and that from the Cebeci model, 20 percent lower.

SSME Full Scale (COCA 4B Test, MPL)

In these tests, the full-scale SSME was regeneratively cooled by two separate cooling loops: one for the combustion chamber out to an area ratio of 5 ($\varepsilon = 5$), the other from $\varepsilon = 5$ to the exit ($\varepsilon = 35$). A predicted wall temperature profile, based on the 3K and 40K scale model results, was used for the BLIMP predictions. The predictions and measurements for each cooling loop and for the entire nozzle are compared in Table 3. It is difficult to determine which model yields the "best" results or what the criterion "best" should be. Using total heat flux or the $\varepsilon = 5$ to $\varepsilon = 35$ section heat flux as a criterion, the Kendall model yields the best results. However, this may be a consequence of errors in the first section predictions.

RL-10 Full Scale, Regeneratively Cooled, $\varepsilon_{exit} = 57$

In this series of eight tests, mixture ratios from 4.5 to 6.0 were used, and both the total heat flux to the walls and some wall temperatures were measured. The results from the Kendall model gave the best agreement with the measurements for all cases — less than 5 percent higher. The results from the Cebeci model, in all cases, were approximately 30 percent lower.

17

TABLE 3. COMPARISON OF PREDICTED AND
         EXPERIMENTAL TOTAL HEAT FLUX
         TO THE WALL FOR SSME, MPL

Model	Combustor to $\epsilon = 5$	$\epsilon = 5$ to $\epsilon = 35$	Total
Kendall	+31%[a]	+3%	+12%
Cebeci	-13%	-30%	-24%
Bushnell	0	-23%	-16%

[a]Values are relative to experimental results —
+31% means that Kendall model predicted 31%
more heat flux than was measured.

In four of these tests, an extension to an area ratio of 205 was added to the RL-10. In these cases, the Kendall model overpredicted the additional heat flux by 200 percent, while the Cebeci model overpredicted by 150 percent. In addition, a velocity profile measured at the exit did not agree with the calculated profile from either model. These differences may result from flow disturbances in the extension section which the models do not consider.

The results from all the hot-fired tests are contradictory, and the "best" turbulence model cannot easily be determined. Complicating factors — mixture ratio, actual wall temperature and pressure, internal flow disturbances — preclude any "untangling" of the information to yield a definite conclusion. The best that can be said is that the Kendall model predicts the highest heat flux, the Cebeci model predicts the lowest heat flux, and the data falls between the two.

The results from the shock tube experiments, which do not have as many complicating factors, favor the Cebeci model. Based on these results and the widespread acceptance of the Cebeci model for other flow situations, the Cebeci model is recommended as the standard model until more conclusive evidence is available. At present, the evidence is not conclusive, and well-defined experiments are needed. However, if overprediction of the heat flux is more desirable than underprediction, the Kendall model should be used. It should also be noted that the degree of uncertainty in predicting the mixture ratio may more than offset differences in the turbulence models.

2.3   SENSITIVITY ANALYSIS

The objective of this subtask was to identify and estimate the importance of the key parameters and physical models within the BLIMP code which could significantly impact the heat flux and thrust loss calculations. A limited number of BLIMP computer runs were made to investigate the sensitivity of the solution to the following models: species diffusion, transport properties, the ideal gas assumption, and the use of REFIT. These models will be discussed in the following subsections.* A summary table is presented in the

_____

*The details of all the models studied here can be found in the BLIMP-J Users Manual (Reference 8).

19

in the last subsection (2.3.5). Since the variations among the turbulence models have been discussed in a previous report (Reference 1), they will not be discussed here. It was not within the scope of this study to readjust the constants in any of the models to fit the data more accurately.

2.3.1 Species Diffusion

The calculation of the species diffusion coefficients is based on the the bifurcation approximation and is described in Reference 8. This approximation was formulated and calibrated for low-pressure gases. Furthermore, there are three different methods of considering diffusion in BLIMP-J: equal diffusion coefficients, unequal diffusion coefficients without thermal diffusion, and unequal diffusion coefficients with thermal diffusion. Therefore, the sensitivity of the results to diffusion modeling was considered from two aspects: the choice of method and the errors in the calculated values of the diffusion coefficients due to inaccuracies in the approximation.

BLIMP-J solutions for the SSME nominal power level (P_c = 20.5 MN/m^2, T_c = 3653°K) were obtained for each of the three methods described above (equal, unequal, and unequal plus thermal diffusion). For the SSME O/H fuel, the three cases differed by less than 1 percent in total heat flux and thrust loss. There were slight differences in the species concentrations at the wall, but these had almost no effect on the results. The simplest method, equal diffusion coefficients, also results in approximately 10-percent savings in computer time. These results for O/H fuel may not be valid for other fuel compositions. Thus, comparisons of the three methods should be performed for each fuel composition considered.

A potential source of error in the model for diffusion coefficients is the unaccounted for effect of high pressures. The effects of pressure on species diffusion are illustrated in Figure 7* (the area of SSME applicability is shaded). This figure shows the ratio of the product of the pressure and diffusivity at the same temperature but a low pressure.[†] The ratio

---

*Reproduced from Reference 6.
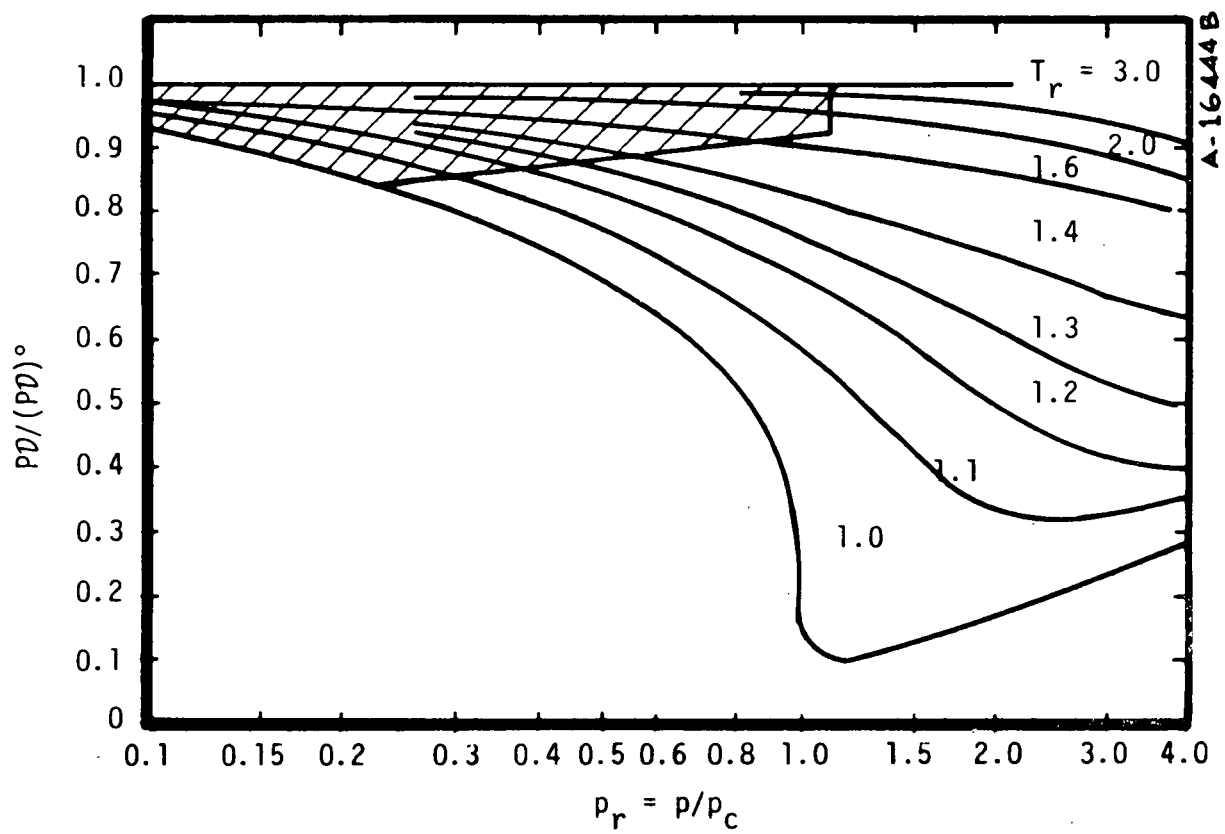[†]Denoted by superscript "°".

Figure 7.   Effect of pressure on self-diffusion coefficient.

is plotted as a function of reduced pressure at several reduced temperatures. It is clear from the figure that the diffusivity of a gas diffusing through itself varies as a function of both pressure and temperature. In order to compute the reduced temperature and pressure (to locate a point on the figure), the mixture critical properties are needed. These values are obtained from the species concentrations and their critical values of pressure and temperature through a mole fraction weighted average:

$$P_c(\text{mixture}) = \Sigma \ y_i P_{ci}$$

$$T_c(\text{mixture}) = \Sigma \ y_i T_{ci}$$

For the hyrogen/oxygen system (as in the SSME) with a mixture ratio of 6, the critical properties are P_c = 15.4, MN/m^2 (153 atm), and T_c = 440°K. For the conditions in the SSME, the effect of high pressure on diffusivity is at most 15 percent (see Figure 7).

Therefore, although the effect of pressure will be to cause a deviation in the diffusion factors, this effect is evidently not transmitted to the calculation of heat flux from the boundary layer, since the three modes of modeling diffusivities showed almost no change in heat flux to the wall. For this reason, the effect of diffusion factor inaccuracies will be negligible.

2.3.2 Transport Properties

The models for thermal conductivity and viscosity are, like that for species diffusion, formulated for low-pressure gases. Therefore, it is considered appropriate to estimate potential variations in the properties by considering the change in value caused by increased pressure. These changes can be calculated in the same manner as described for species diffusion. Figures 8 and 9* give the reduced viscosity and conductivity as functions of reduced temperature and pressure. For the region of SSME operation, the deviation from the low-pressure values is seen to be less than 5 percent.

For the sensitivity analysis, a 20-percent variation in both conductivity and viscosity was considered. The effects of these variations in

---

*Reproduced from Reference 6.
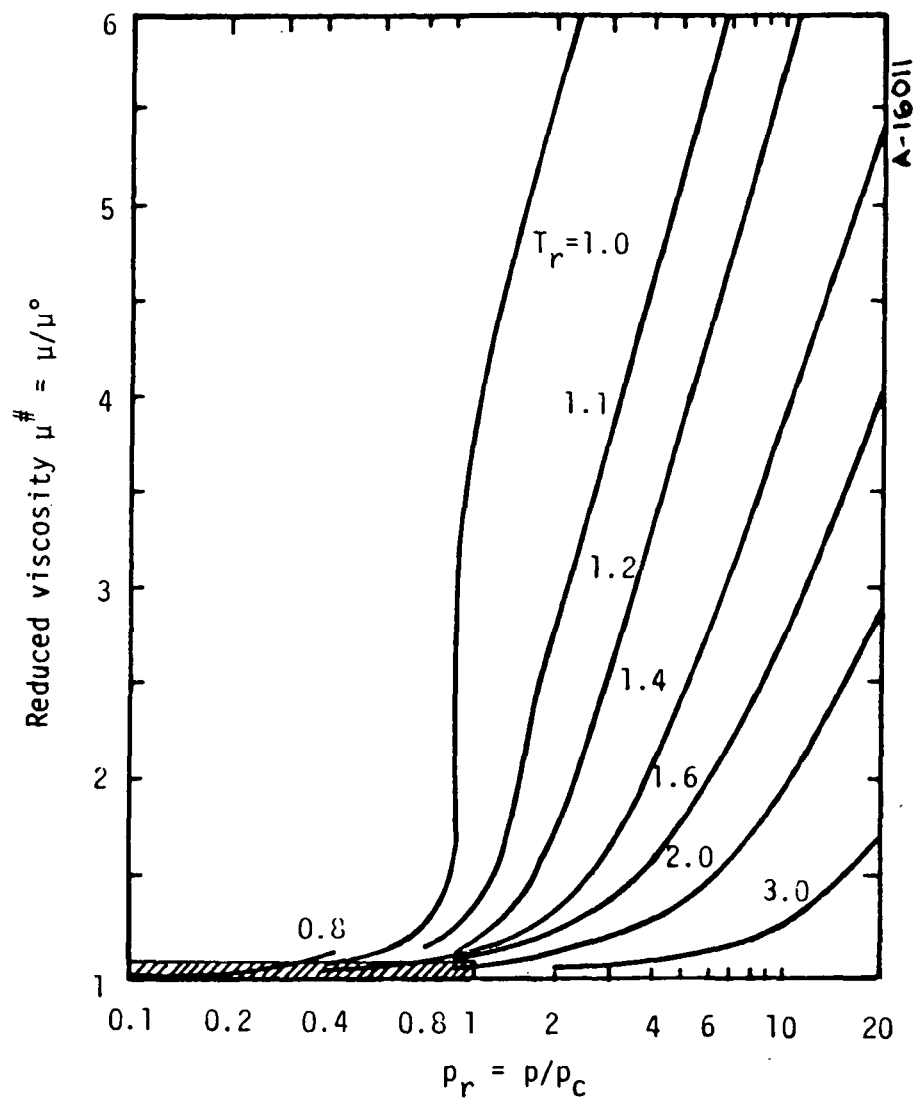
Figure 8. Influence of high pressure on molecular viscosity.
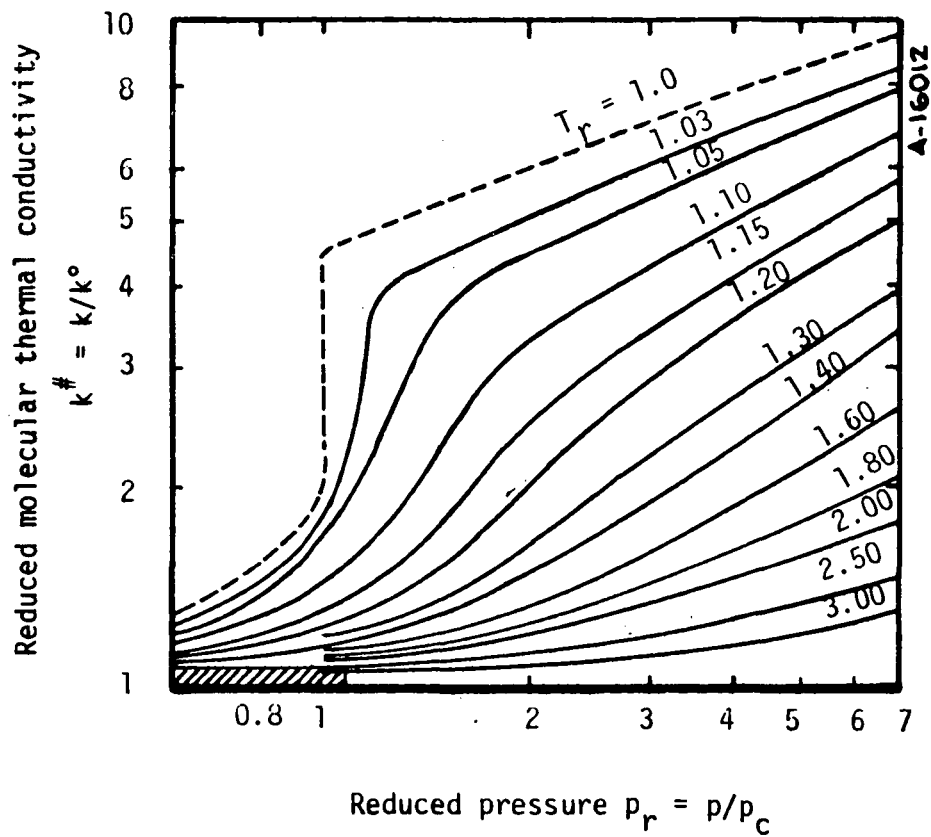
Figure 9. Influence of high pressures on
molecular thermal conductivity.

viscosity and conductivity on the heat flux and thrust loss are shown in Figure 10 and Table 4. The thrust loss is calculated at the exit plane of a 10°/10° converging-diverging nozzle. Figure 10 gives the percent difference in heat flux from the nominal value as a function of boundary layer running length for the cases in Table 4. The conductivity variation has considerably more effect than the viscosity variation. The effect on heat flux to the wall is always less than the 20-percent variation in the conductivity itself. Since a 20-percent variation in viscosity and conductivity produces around 10-percent variation in heat flux to the surface, the maximum of 5-percent change caused by high pressure effects results in less than 2- to 3-percent change in heat transfer. Similarly, these effects result in less than 2-percent change in the thrust loss at the exit. Therefore, the low pressure models for viscosity and conductivity are adequate.

2.3.3 Ideal Gas Model

The predictive accuracy of the analytical model based on the ideal gas law (which describes the behavior of a chemically-reacting mixture) depends strongly on temperature and pressure. When temperatures are high and pressures are low, the ideal gas law has been experimentally verified to be a good approximation. But when temperatures are low and pressures are high, the ideal gas law no longer governs the behavior of the gas mixture and the particle interaction phenomenon, not described by the ideal gas law, becomes significant. Another equation of state that considers such phenomenon should then be used. When both temperature and pressures are high, it has not been determined whether an equation of state which accounts for the high pressure effects is necessary. Therefore, the following sensitivity study was performed to evaluate the high pressure effects at the conditions of interest.

Sample calculations were made using the high pressure version of the ACE (Aerotherm Chemical Equilibrium) computer code. This version of the ACE code uses the Van der Waal's equation, shown below, to describe the state of the reactive gas mixture

$$P_j = \frac{RT}{V_j - b_j} - \frac{A_j}{V_j^2} \tag{3}$$
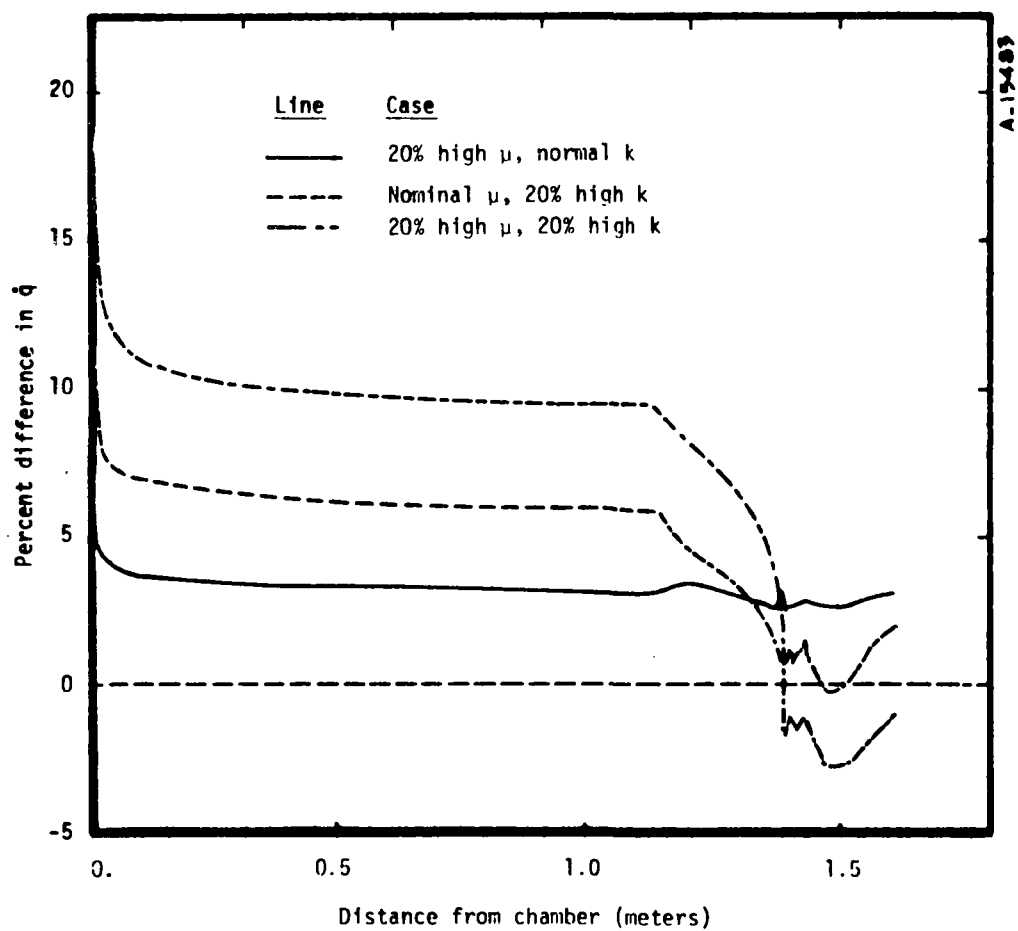
Figure 10. Comparison of effects of variation in viscosity and conductance on q̇ JPL 10°/10° CD nozzle.

TABLE 4. EFFECT OF VARIATION OF μ AND k
ON THRUST LOSS — JPL 10°/10° CD
NOZZLE

		$\underline{\Delta F}$
$\mu = \mu_{NOM}$	$k = k_{NOM}$	20.02 lb_f
$\mu = 1.2\ \mu_{NOM}$	$k = k_{NOM}$	20.17
$\mu = \mu_{NOM}$	$k = 1.2\ k_{NOM}$	20.95
$\mu = 1.2\ \mu_{NOM}$	$k = 1.2\ k_{NOM}$	21.66

The quantities A_j and b_j are constants for each species. The term A_j/V_j^2 accounts for an attractive pressure which arises due to attractive interaction forces among the molecules, whereas b_j is a constant roughly indicative of the volume occupies by the molecules themselves. The constants A_j and b_j are generally determined through the following relationships:

$$A_j = \frac{27}{64}\frac{R^2 T_{cj}{}^2}{P_{cj}} \quad , \quad b_j = \frac{RT_{cj}}{8P_{cj}} \tag{4}$$

where T_{cj} and P_{cj} are the critical temperature and pressure of species j.

The procedure to determine the thermodynamic properties is somewhat more complicated than the procedure that is used for the ideal gas law. The major equations that are used in the code are highlighted as follows:

$$(H_j - H_j^\circ)_T = \int_0^P \left[V_j - T\left(\frac{\partial V_j}{\partial T}\right)_p \right] dP \tag{5}$$

$$(S_j - S_j^\circ)_T = \int_0^P \left[\frac{R}{P} - \left(\frac{\partial V_j}{\partial T}\right)_p \right] dP - R \ln P \tag{6}$$

$$\left(C_{p_j} - C_{p_j}{}^\circ \right)_T = T \int_0^P \left(\frac{\partial^2 V_j}{\partial T^2} \right)_p dP \tag{7}$$

$$(G_j - G_j^\circ)_T = RT \int_0^P \left(\frac{V_j}{RT} - \frac{1}{P} \right) dP \tag{8}$$

The variables on the left-hand side of the equations with "°" designations are the thermodynamic properties at the desired temperature* but at low

---

*The subscript "T" is used to denote evaluation at the same temperature.

28

pressure. Therefore, the terms on the right-hand side of the equations account for the high pressure effects on the thermodynamics properties.

The reactive gas mixture for the calculations is a hydrogen and oxygen mixture with a mixture ratio of 6. The critical temperatures and pressures that were used for the calibrations are tabulated in Table 5. Those species for which the critical properties were not available were treated as ideal gases by arbitrarily setting A_j and b_j to zero. These species typically account for less than 5 percent of the moles in the mixture, therefore, this assumption has a small impact on the calculation.

TABLE 5. CRITICAL PROPERTIES OF H/O MIXTURE

	Critical Pressure (MN/m^2)	Critical Temp (°K)	Mole Fraction[a]
H_2	1.297	33.24	0.2484
H	--	--	0.0287
HO	--	--	0.0400
HO_2	--	--	--
H_2O	22.26	647.27	0.6773
H_2O_2	--	--	--
O	--	--	0.0027
O_2	5.08	154.78	0.0029

[a]This is the composition predicted for an ideal mixture of ideal gases at mixture ratio of 6 for the SSME motor at chamber conditions (P = 20.2 MN/m^2, T = 3653°K)

Figure 11 shows the results of the sample calculations. The enthalpy and molecular weight of the gas mixture, calculated using the Van der Waal's equation, were compared to those calculated using the ideal gas law. For the molecular weight predictions, both models predicted the same result throughout the temperature range, indicating that the composition is not significantly changed. At reduced temperatures above 2 (T above 1000°K), the ideal gas and Van der Waal's models predict the same enthalpy, as shown in Figure 11, but at lower reduced temperatures some deviation occurs.
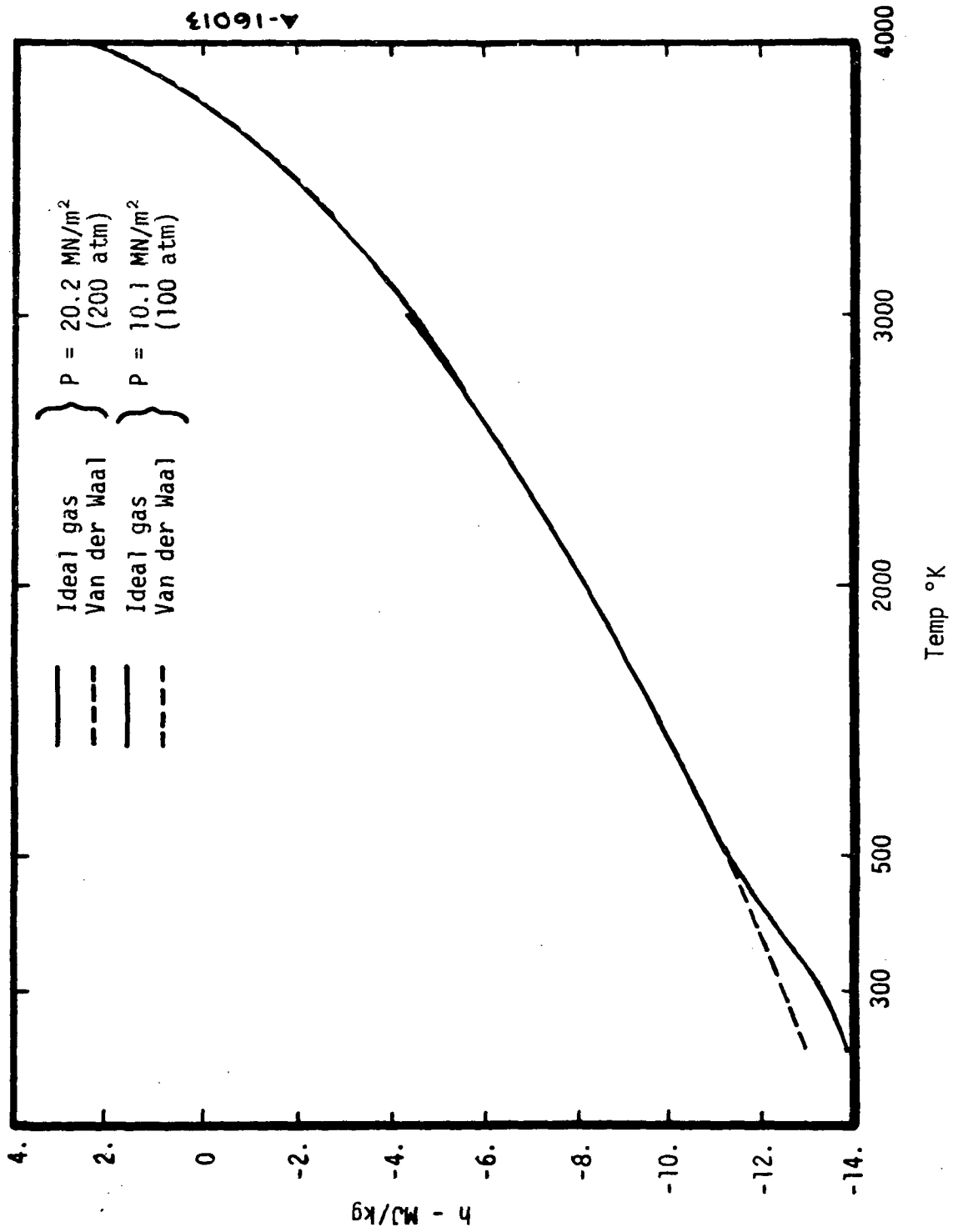
Figure 11. Comparison of enthalpy for ideal gas and Van der Waal's gas.

30

Figure 12 shows the range of reduced temperature and pressure for the SSME applications. It should be noted that the smallest reduced temperatures occur at very low values of reduced pressure where the ideal gas law holds.

As a further check on the validity of the ideal gas approximation, experimental results for the deviation from ideal gas behavior were compared to the range of pressure and temperatures for SSME operation. Figure 13* shows the compressibility factor ($Z = P/\rho RT$) derived from experimental data and indicates the range of applicability. It is clear that Z will remain close to unity (ideal gas) throughout the SSME range and that deviations from ideal gas behavior are small.

The use of Van der Waal's equation was dictated by two factors: it is probably the easiest extrapolation from ideal behavior to implement, and we have a version of ACE which includes Van der Waal's equation. Use of the equation is not meant to imply that Van der Waal's model is completely accurate over the whole range of pressures and temperatures of interest, however, it is an indicator of nonideal behavior. Since there were no significant deviations from ideal gas behavior, the Van der Waal's was not used further.

2.3.4 REFIT Option

The nodal REFIT option adjusts the location of the nodes across the boundary layer in an attempt to maintain optimum definition of the velocity profile. Recommended values of the parameters that control this option are built into the BLIMP program. The purpose of this study was to evaluate the impact of the REFIT option on the wall heat flux ($\dot{q}_w$), the momentum thickness (θ), and the thrust loss (ΔF).

The advantages of the REFIT option are:

● The number of nodes (and the execution time) necessary for problems with a high degree of profile shape change (e.g., turbulence, nonsimilar wall effects, and pressure gradients) is reduced

---

*Reproduced from Reference 7.

Figure 12. Reduced temperature and pressure regime for SSME application.
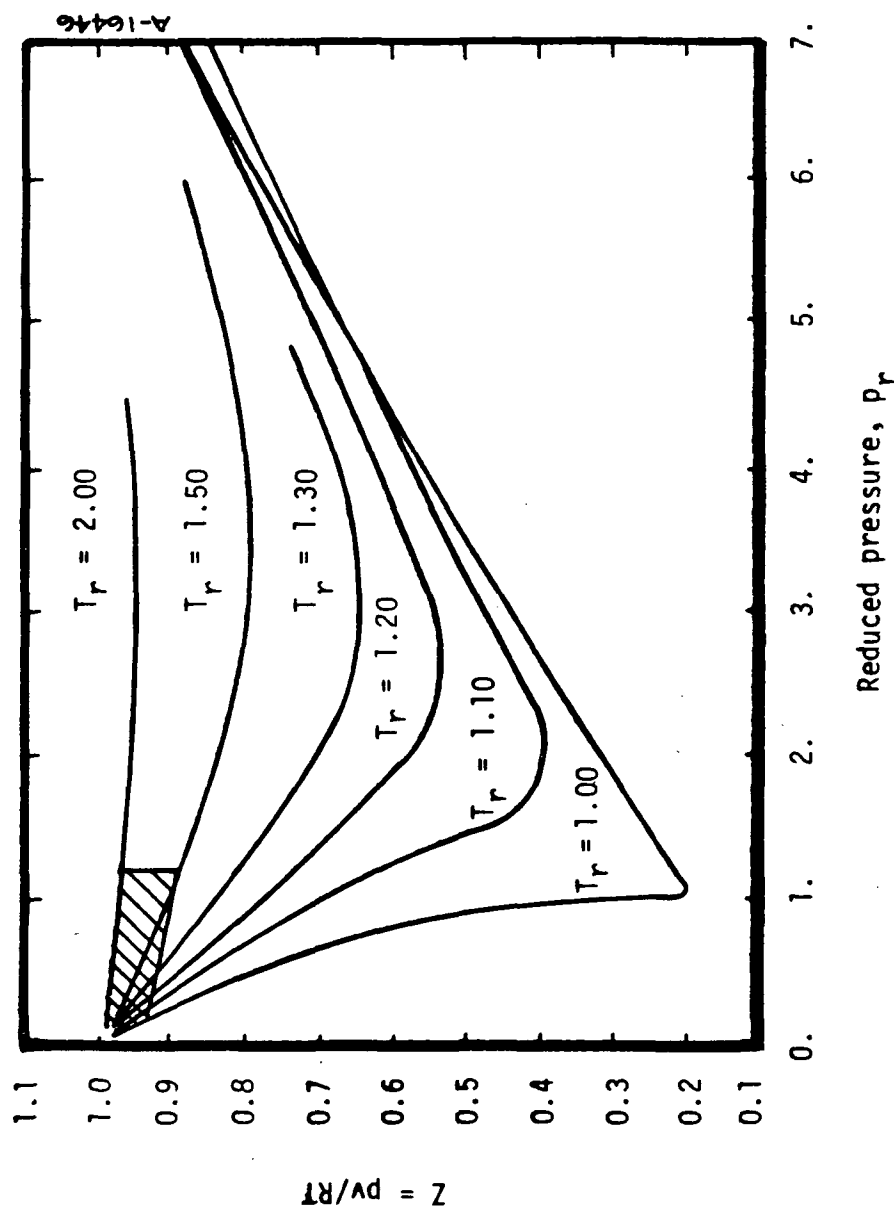
Figure 13. Effect of pressure on compressibility (curves based on experimental results).

33

- The user does not need to guess beforehand how the nodes should be placed to adequately describe the profile over the entire streamwise length

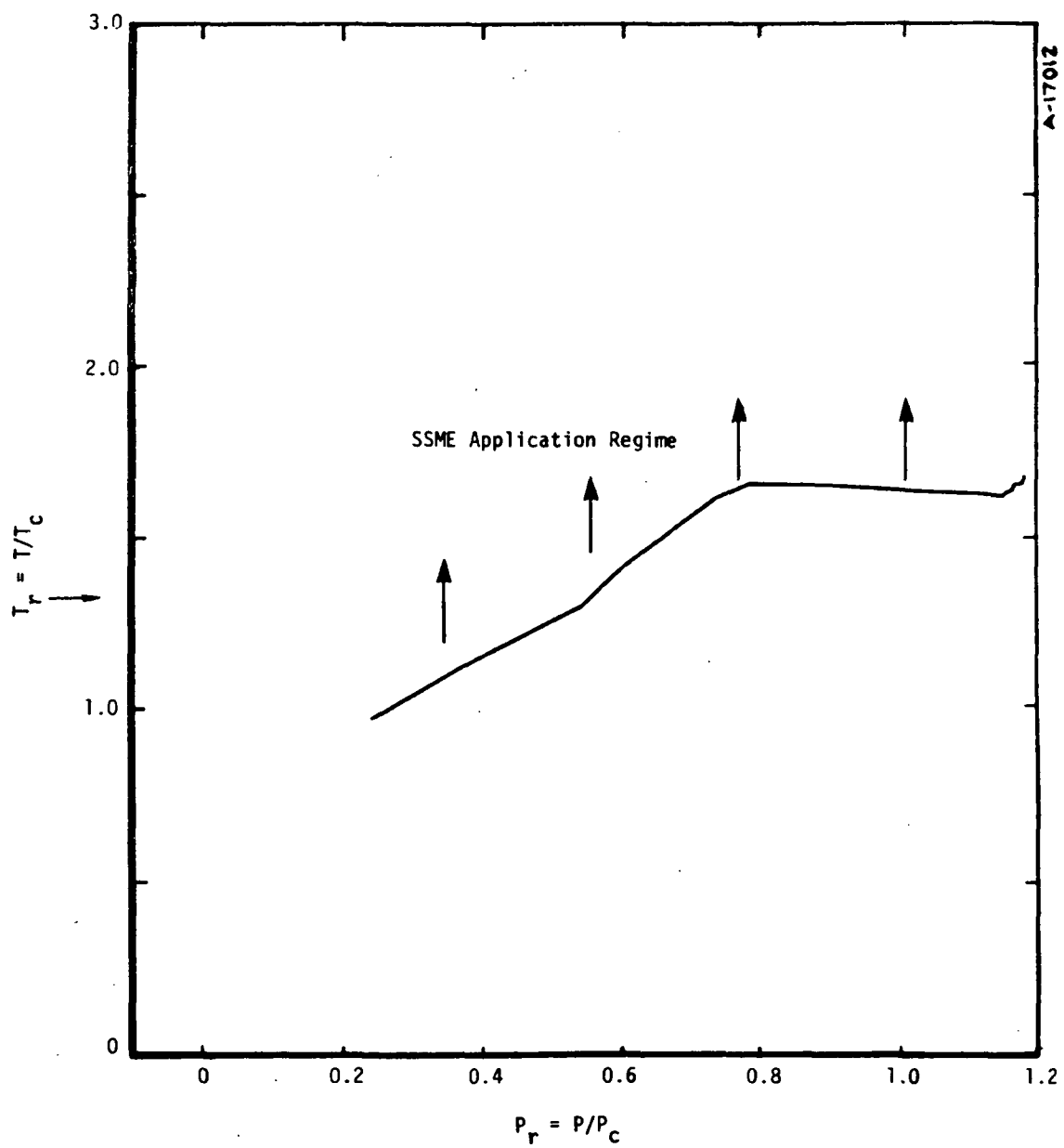This second advantage is the most important and offers the greatest benefit to the user. It is very difficult to choose the optimum placement of the nodes a priori, and therefore, REFIT is invaluable in making appropriate adjustments to the node placement. We strongly recommend using this option.

However, the REFIT procedure does have one major disadvantage — it introduces a slight numerical inaccuracy into the solution. This can be detected by comparing a solution using REFIT to one which does not use REFIT, but which uses an optimal node placement selected with the aid of REFIT. In general, this minor inaccuracy amounts to less than 10 percent in $\dot{q}_w$ and less than 2 percent in θ and ΔF for the entire body length. In most cases, the results for $\dot{q}_w$, τ_w, and ΔF with REFIT are lower than the "NO REFIT" results. For example, for the flat plate with low speed airflow, the momentum transfer coefficient ($C_f/2$) is reduced from its NO REFIT value by about 10 percent over a five order of magnitude change in Re_θ.

To illustrate the effect of REFIT on a solution, the Nerem shock tube flow case was run with several values of the REFIT parameters. The results for $\dot{q}_w$ are shown in Figure 14 and clearly indicate the slight drop in $\dot{q}_w$ after each REFIT. This drop is typical, and the cumulative effect is generally less than 10 percent. Changes in the REFIT parameters may also change the number of REFIT stations and the magnitude of the differences (as can be seen in Figure 14); however, this effect is small.

As a second test of the effects of REFIT, results of the SSME prediction (Sample Case 1 in the BLIMP-J User's Manual (Reference 8)) with and without REFIT were compared. The recommended REFIT parameters with 12 nodes were used for the REFIT case, resulting in REFIT being called six times over the entire length of the nozzle. For the NO REFIT case, 14 nodes were used, with the location of the nodes selected to satisfy both the upstream and downstream conditions. (This selection was greatly aided by the examination of the results from the REFIT case.) The REFIT results for $\dot{q}_w$ were less than 10 percent below the NO REFIT results. The momentum thickness and thrust loss were within 2 percent for the two cases. The execution time for the NO REFIT case was about 5 percent more than the REFIT case.
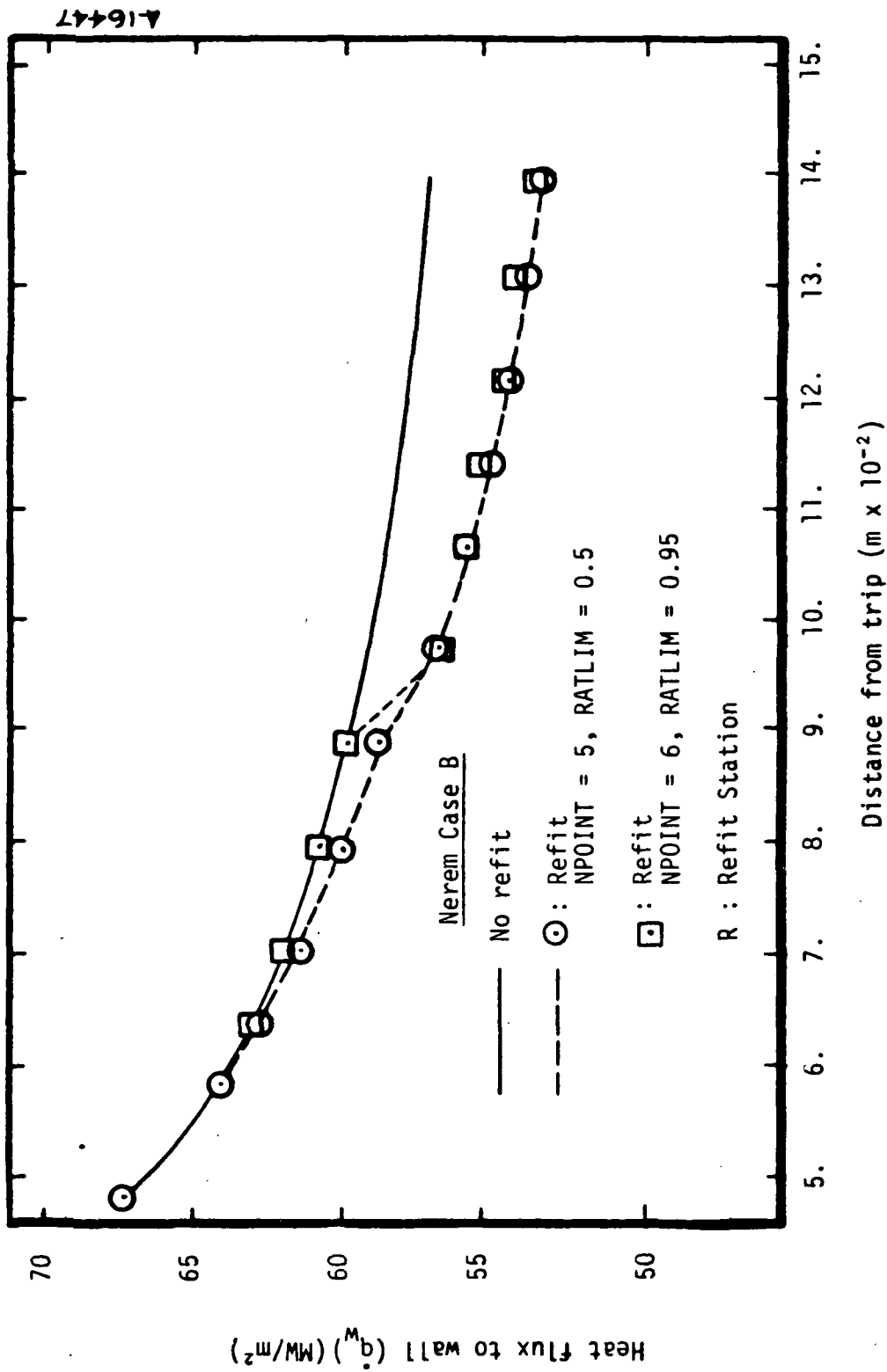
Figure 14. Effect of REFIT on wall heat flux.

35

It should be emphasized that the results of this study strongly support the use of the REFIT option, particularly for preliminary runs where the slight loss in accuracy is compensated for by the use of the built-in nodal distribution. Knowledge of the velocity profile gained from the preliminary runs can then be used to select an adequate nodal distribution for the NO REFIT case in those cases where extreme accuracy is required. A procedure for this use of the REFIT option is given in Appendix B.

2.3.5 Summary

A short summary of the sensitivity analysis is provided in the following table. This table gives the approximate effect on heat flux and thrust loss for the four models investigated.

TABLE 6. ESTIMATED SENSITIVITIES

Variational Model/Effect ON	Heat Flux	Thrust Loss
±10% in Species Diffusion	<3%	<1%
±10% in Transport Properties		
Viscosity	<4%	Negligible
Conductivity	<8%	<5%
Ideal Gas	Negligible	Negligible
REFIT	<10%	<2%

36

SECTION 3

TEST PROGRAM

The purpose of this task was to determine an experiment which would result in data sufficiently accurate to illustrate the differences among the three turbulence models currently in BLIMP-J. It was shown in the previous section that there is little complete experimental heat flux data for highly cooled turbulent boundary layers, yet only these boundary layer conditions show the differences among the predictions of the turbulence models.

To study these highly cooled boundary layers, two experimental arrangements, a 10°/10° converging/diverging nozzle and a flat plate* were examined. The BLIMP-J code was used to predict the model-produced differences at the desired conditions to insure that significant differences would be apparent. (A large difference between the model predictions of heat flux is desirable to overcome the inevitable data scatter and experimental error bands.)

A description of the general experimental conditions and the specific apparatus follows. Throughout this section the differences between the predictions of the Kendall model and the Cebeci model are used to indicate the model-produced heat flux differences.

General Experimental Conditions

The experimental conditions must guarantee turbulent flow with large property variation (density, viscosity, conductivity, and static temperature) near the wall (cold wall/hot flow), and at the same time ensure the accuracy and survivability of measuring instruments.

---

*Experimentally, axial flow down a hollow cylinder is equivalent to flat plate flow as long as the boundary layer is very small compared to the inside radius of the cylinder.

To ensure turbulent flow, length Reynolds numbers (Re_x) larger than 3×10^6 are recommended. This will not only minimize transition effects but will also provide a flow regime most suitable for comparing the turbulent models. Either natural or artificial (a turbulent trip) transition is acceptable. However, since the models are not intended to predict transition effects, the measurement stations should be sufficiently far downstream of any suspected transition effects. Large unit Reynolds number ($\rho_e u_e/\mu_e$) flows will have relatively short transition regions and are, therefore, preferred.

The large property variation is maintained (cold wall in a hot flow) by an edge-to-wall temperature ratio larger than 5. The cold wall will localize the property variation near the wall and also closely model SSME behavior. No condensation can be allowed. For facilities where a change in water temperature is used to determine the heat transfer to the wall, a wall temperature of 295°K (530°R) is representative, implying an edge temperature of approximately 1475°K (2655°R).

If these temperatures are unobtainable, cryogenically cooled walls should be considered. For instance, since liquid nitrogen coolant will boil at 77°K, the edge temperature could be approximately 386°K (695°R). But the mass of liquid nitrogen caused to boil by heat transfer to the wall must be determined to calculate the heat flux to the wall. This can be very difficult. If other variables such as wall shear or profiles can be measured or if heat flux can be measured by other means, then cryogenic walls could be used. In this case, condensation on the wall must be avoided; therefore a very dry gas must be used (for instance argon or nitrogen gas).

Pressure gradients large enough to cause laminarization should be avoided. The flat plate configuration has the advantage of isolating the influence of the temperature differences from any pressure effects. However, since the turbulence models have been verified for moderate pressure gradients, the additional complexity of a pressure gradient in a nozzle is probably not critical as long as laminarization does not occur. Other complicating factors such as wall roughness, gross freestream turbulence and swirl should also be avoided.

To use BLIMP to predict the turbulent boundary layer conditions, the following data are necessary. The chamber temperature and pressure must be known, the wall temperature and pressure distributions must be measured, and the wall heat flux or shear or velocity and temperatures profiles must be determined. A turbulent profile upstream of the other measurements would provide detailed initial conditions and make the calculations more accurate. If this is not possible, it becomes more important to minimize the effects of the transition region on the measurements.

For the profile measurements, traversing pitot probes of very thin aperture and traversing thermocouples are needed. An upstream pressure tap and thermocouple are needed for actual chamber conditions. Static pressure taps and thermocouples should be located along the wall. Heat flux could be measured either by coolant temperature rise or wall calorimeter.

Finally, the instruments that measure the desired properties of the boundary layer (pitot probes, thermocouples) must be able to withstand the stagnation conditions in the boundary layer and freestream flows.*

Nozzle Flow

Figure 15 shows the difference in predictions for the Cebeci and Kendall models on the 10°/10° CD nozzle with wall temperature of 333°K. The chamber pressure is 1.01 MN/m^2 (10 atmospheres) and the chamber temperature has been varied from 1111°K (2000°R) to 1667°K (3000°R). Higher chamber temperature implies higher edge temperature and a higher difference in the predicted heat fluxes.

The difference between the models is clearly evident for the nozzle flows in Figure 15 for the converging part of the nozzle. The diverging part of the nozzle does not show significant differences among the models since the edge to wall temperature ratio is too low.

---

*However, velocity profiles could be obtained from laser velocimetry, and temperature profiles could be measured spectroscopically, thereby eliminating the survivability problem.
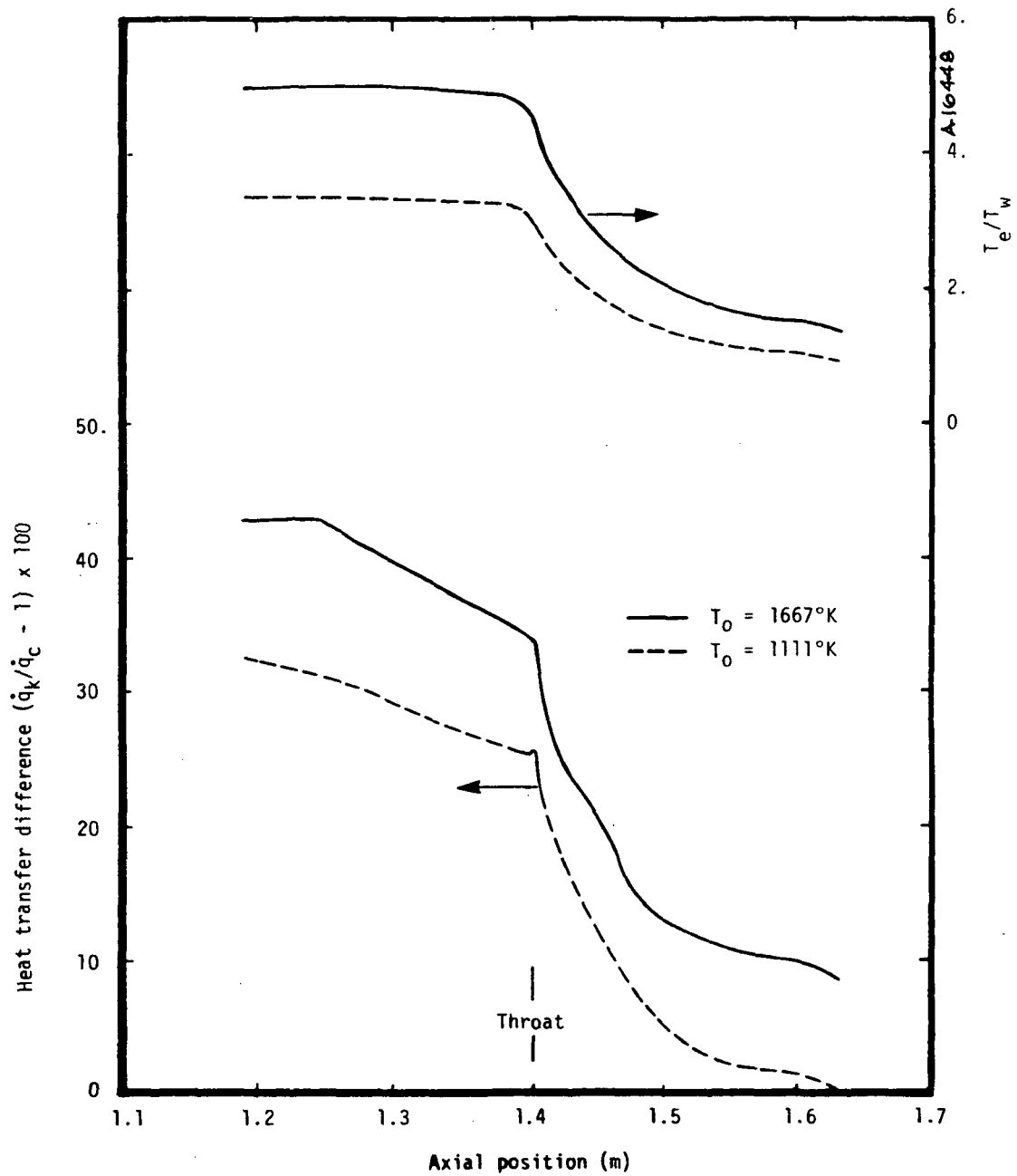
Figure 15. Effect of chamber temperature on heat flux
difference and edge temperature (10°/10°
CD nozzle).

Flat Plate*

Flat plate test conditions suitable for testing the turbulent models were also examined. For relatively low speed flow (edge Mach number = 0.3) of air over a plate at 333°K, the Kendall and Cebeci predictions of heat transfer to the wall differed by up to 40 percent for T_e/T_w = 4.9.

Two chamber pressures (1 and 10 atmospheres) and two chamber temperatures (1111°K and 1667°K) were examined. For the low pressure cases, the flow began transition at around 0.21 meters (0.7 feet) (Re_θ, trans = 360), whereas at high pressure the flow became turbulent very close to the sharp leading edge. All the high pressure calculations were therefore run with immediate transition ("fully turbulent").

The effects of natural transition on the low-temperature, low-pressure calculations were investigated further. Two runs were made: one low pressure, low temperature, and natural transition at Re_θ = 360, and another with low pressure, modeling a rough leading edge — fully turbulent at the start of the boundary layer. Both runs, natural transition and fully turbulent, were continued out to 1.820 meters (6 feet) and the differences in the two turbulent models were examined. Model-produced differences are shown in Figure 16. The predicted heat transfer at 0.914, 1.219, and 1.829 meters (3, 4, and 6 feet) for the Kendall model is shown in Table 7.

TABLE 7. PREDICTED HEAT TRANSFER FOR LOW PRESSURE FLAT
PLATE (KENDALL MODEL)

(P_{stag} = 0.101 MN/m^2, T_{stag} = 1111°K, Re' = 1.35 x 10^6/m)

x Running Length (meters)	$\dot{q}$ Natural Transition (MW/m^2)	$\dot{q}$ Fully Turbulent (MW/m^2)
0.914	0.1263	0.1212
1.219	0.1187	0.1154
1.829	0.1096	0.1074

*The flat plate results also apply to flow inside a cylinder, as in the Nerem and Hopkins experiments.
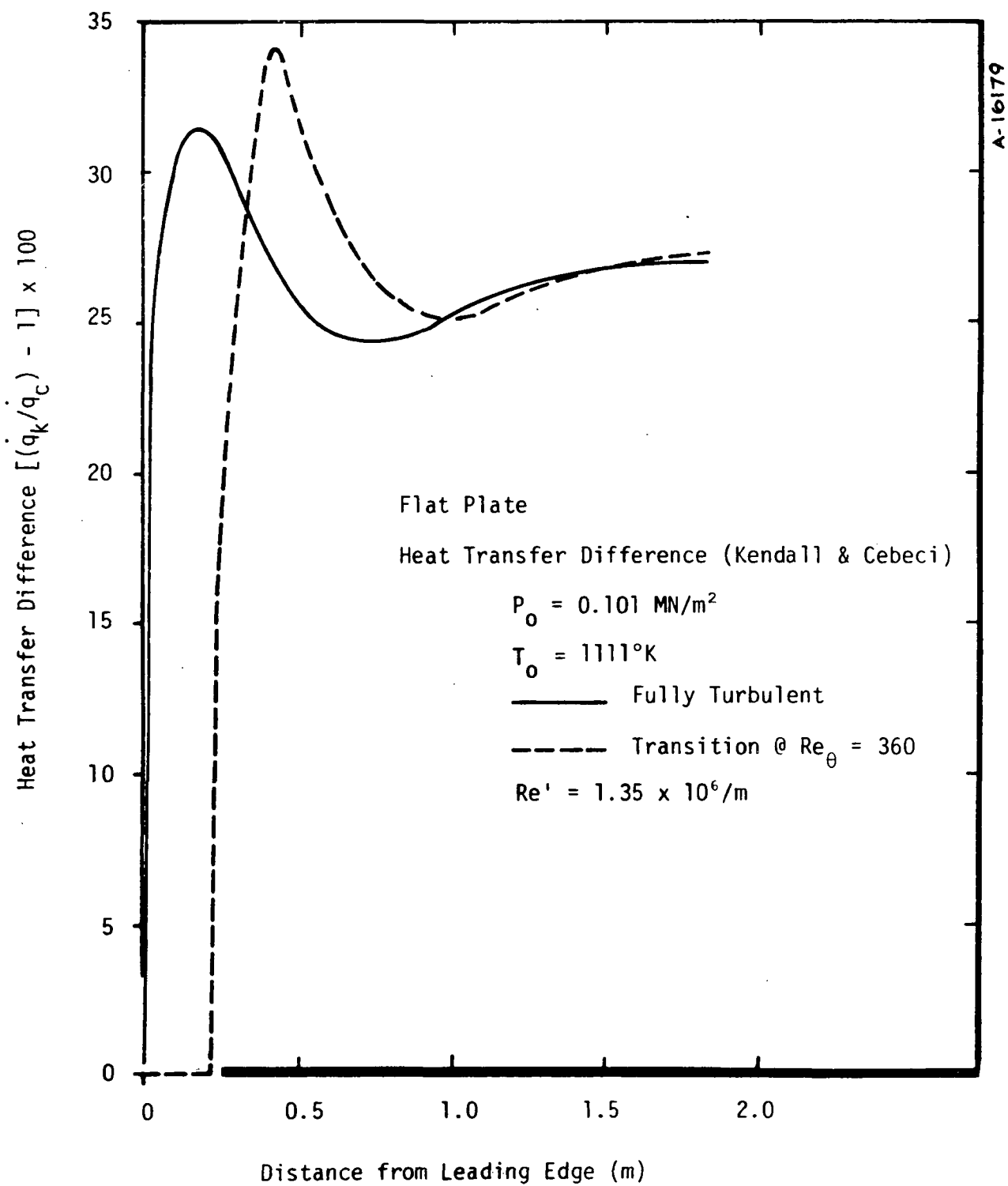
Figure 16. Effect of transition location on heat transfer differences.

Vertical axis: Heat Transfer Difference $[(\dot{q}_k/\dot{q}_c) - 1] \times 100$

Horizontal axis: Distance from Leading Edge (m)

Flat Plate

Heat Transfer Difference (Kendall & Cebeci)

$P_o = 0.101$ MN/m^2

$T_o = 1111°$K

———— Fully Turbulent

– – – – Transition @ $Re_\theta = 360$

$Re' = 1.35 \times 10^6$/m

A-16179

The results of Table 7 and Figure 16 show that the test may be run with either a roughened or a smooth leading edge as long as sufficient running length is provided, so that data is taken well past transition. (For the same conditions except at a stagnation pressure of 1.0 MN/m² (10 atm), the two runs are identical after roughly 0.01 meters. This illustrates the advantage of having a large unit Reynolds number.)

The effects of chamber conditions are shown in Figures 17 and 18. As shown in the figures, the higher the chamber temperature, the greater the difference in the heat transfer predicted by the Kendall and Cebeci models. The best conditions are those that give the largest difference between between the models, since that reduces the possibility of scatter in the data leading to inconclusive comparisons.

Test Recommendation

To show the greatest differences in model predictions, the following test conditions should be used. The highest possible chamber pressure (10 atmospheres would be sufficient) and temperature 1389°K (2500°R) should be used for either a nozzle or flat plate. This will produce the highest Reynolds numbers and quickest transition and therefore the most extensive area of turbulent flow. To avoid nonequilibrium chemistry effects, the gas used should not be reactive. Instrumentation should include static pressure taps on the nozzle and thermocouples on the wall, as well as a traversing pitot probe and a thermocouple at one or more positions where the flow is fully turbulent.

There are advantages and disadvantages for both flow situations. Since it is easier to generate high pressure in an internal flow device than on a flat plate, pressure considerations probably favor an internal flow situation. The nozzle will act as a flow containment vessel. If the effects of pressure gradient were to be isolated from the flow, zero pressure gradients could be generated with a cylinder instead of a contoured nozzle. However, at atmosphere pressure, a flat plate arrangement might be more convenient to instrument.

The suggestions offered here are intended to serve as guidelines for the type of data and flow conditions that would be most useful. The final selection
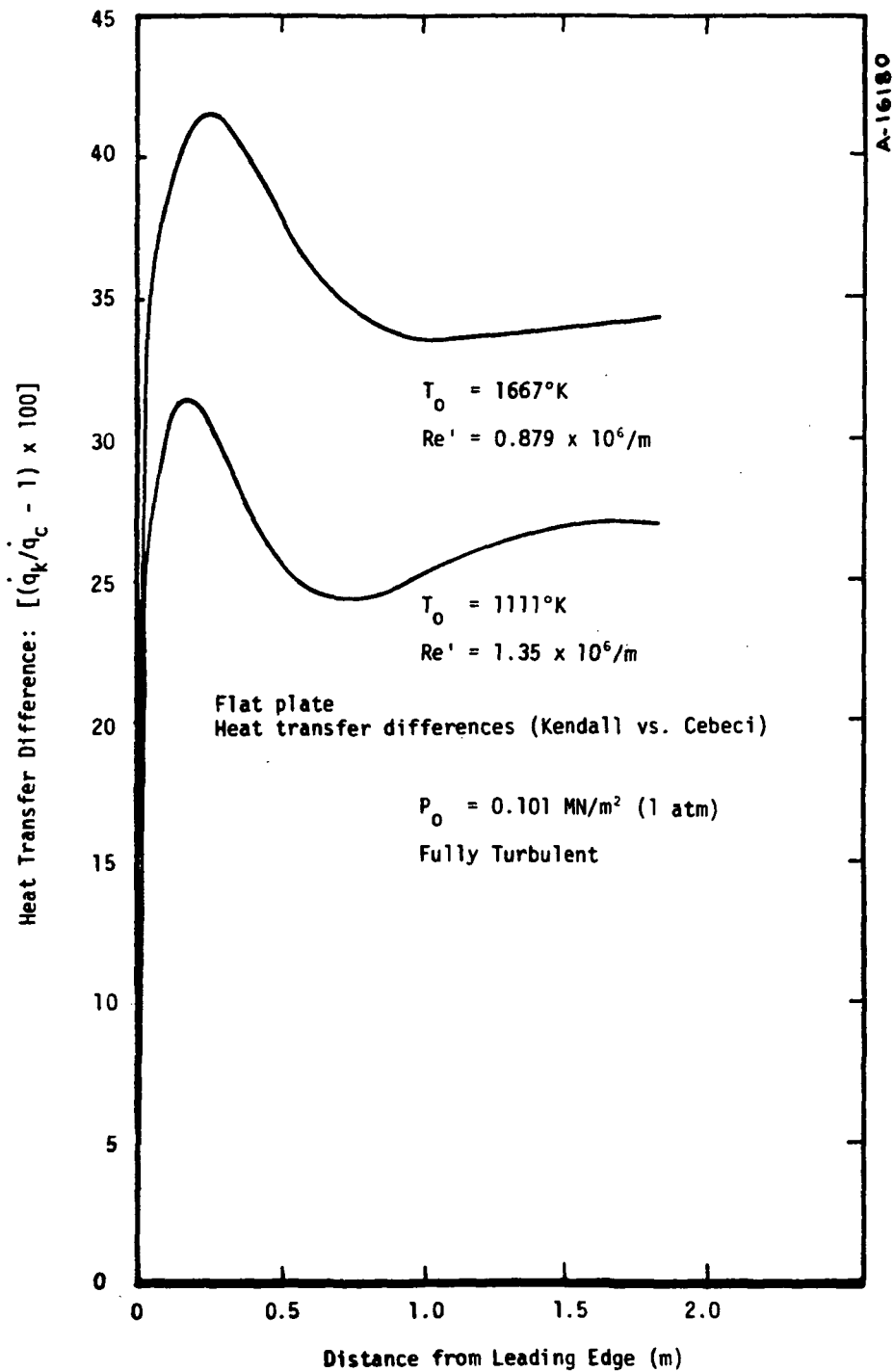
Figure 17. Effect on heat transfer differences of chamber temperature at low pressure.

The y-axis is labeled "Heat Transfer Difference $[(\dot{q}_k/\dot{q}_c - 1) * 100]$" and the x-axis is labeled "Distance from Leading Edge (m)".

Upper curve annotations:

$T_0 = 1667°K$

$Re' = 8.79 \times 10^6/m$

Lower curve annotations:

$T_0 = 1111°K$

$Re' = 1.35 \times 10^7/m$

Flat Plate
Heat Transfer Differences (Kendall vs. Cebeci)

$P_0 = 1.013 \ MN/m^2$ (10 atm)

Fully Turbulent

4-16181
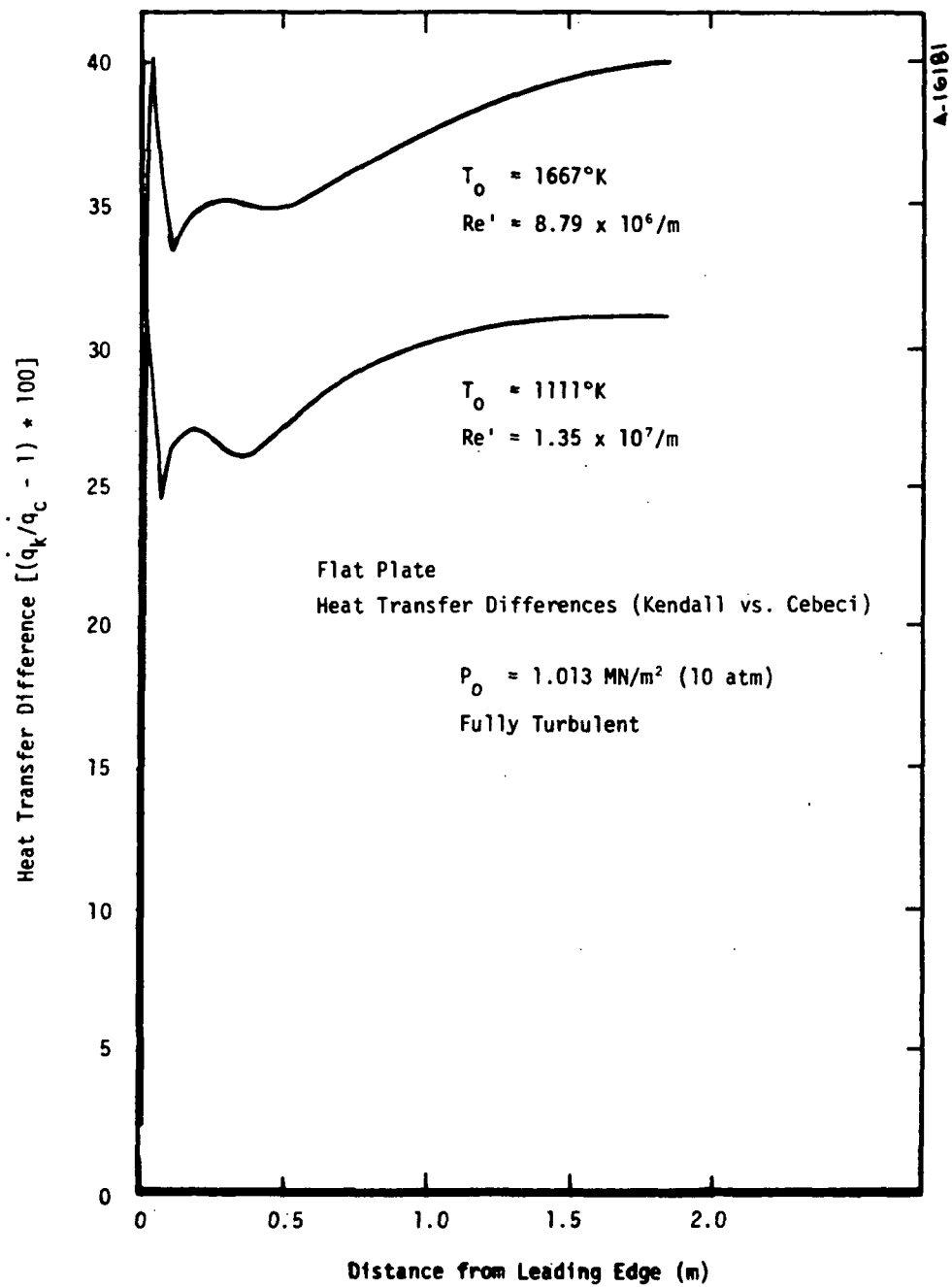
Figure 18.   Effect on heat transfer difference
of chamber temperature at high pressure.

45

of a test arrangement will probably depend on the capability of existing facilities to best meet the experimental objective.

Approximate costs for these tests (if done at a facility similar to the JPL facility) are estimated at $100K to $125K, not including the cost of the basic facility (instrumented nozzle or plate, probes, traversing equipment, etc.). The cost includes some equipment modification for the specific test conditions, some new equipment, calibration and checkout, testing, data reduction, and analysis.

SECTION 4

REACTION KINETICS

The objective of this task was to determine if gas phase chemical reaction kinetics significantly influence boundary layer behavior in an oxygen/ hydrogen liquid propellant rocket engine. There are two possible sources of kinetic effects: the edge conditions and the boundary layer flow itself. The boundary layer effects can in turn be broken into the effect of energetics differences, and chemistry differences. To achieve the objective, the RL-10 nozzle with large expansion ratio was studied. An ODK (one-dimensional kinetic expansion) run at mixture ratios of 0.5, 2, 5, 8 and 12 provided the axial pressure distribution and composition for the kinetically controlled edge conditions.

The first task was to run the version of BLIMP with chemical kinetics (KBLIMP). However, the kinetics package in KBLIMP is not satisfactory for high pressures and near-equilibrium conditions, and it failed. Near equilibrium the rate of reaction is determined by subtracting two nearly equal numbers, the forward and backward reaction rates. This particular formulation has computational problems in cases like that; vast amounts of computer time are consumed without much success. Since replacing the kinetics package in KBLIMP is a major effort, the attempt to run a kinetically-controlled boundary layer solution was abandoned.

The other way to analyze the effects of kinetics on the boundary layer flow is to examine the core flow for kinetics and estimate the effect of changing edge conditions on the flow in the boundary layer. To this end, an equilibrium isentropic expansion at the kinetic pressures and total enthalpy was calculated by the ACE* program. There are two different methods of

---

*Aerotherm Chemical Equilibrium.

computing the edge conditions in BLIMP: nonisentropic and isentropic. The nonisentropic is least common, requiring the input of the axial pressure and velocity distributions. From the chamber (total) enthalpy and local velocity, a static enthalpy is computed, which, along with the pressure, determines the edge conditions. The more usual method of calculating edge properties is with only a pressure distribution. Knowing the pressure and assuming the same entropy as in the chamber allows determination of the edge state, from which a velocity is calculated. Since the second method is the more commonly used method in BLIMP, it was also used for the ACE calculations. The results of this equilibrium expansion, at constant entropy with kinetic pressures, are discussed below.

Table 8 shows that in the chamber and at the throat, the composition is essentially in equilibrium for all mixture ratios, thus there are no kinetic effects in the edge up to the throat. This is because the high pressure and temperature and low velocity make reactions fast compared to the flow velocity. The expansion also shows that for fuel rich (mixture ratio = 2 or 5) or oxidizer rich (mixture ratio = 12) cases there are no significant kinetic effects, even at the exit plane. This can be seen by comparing the mole fractions of H_2O for the kinetic and equilibrium runs. For example, in the fuel-rich cases (mixture ratio = 2 or 5) at the exit plane, the equilibrium predictions both show H_2O and an excess of fuel (H_2). But, examining the difference in the amounts of water predicted kinetically and at equilibrium shows that there is very little difference between the two. This indicates that most of the oxidizer that is available has been consumed, even in the kinetic case. The reactions go to completion in the chamber and very little 0 or O_2 is left to react as the flow proceeds down the nozzle. Therefore, the equilibrium and kinetic edge conditions are approximately the same.

The same arguments can be applied to the oxidizer-rich case (mixture ratio = 12) interchanging the H and H_2 species. Here there is a slightly larger effect than the two fuel-rich cases, but still not significant (5 percent change in H_2O concentrations).

This conclusion is probably true for other propellants in the fuel-rich or oxidizer-rich cases. The reasons are the high pressures and temperatures of the chamber, and an excess of one reactant. The high temperature will cause the

48

TABLE 8. EFFECT OF MIXTURE RATIO ON COMPOSITION
(MOLE FRACTION) AT CHAMBER, THROAT AND EXIT

Mixture Ratio = 2.

Species	Chamber		Throat		Exit	
	Kinetic	Equil.	Kinetic	Equil.	Kinetic	Equil.
H	0.18351-3	0.18359-3	0.10911-3	0.35256-4	0.10369-3	0.10369-3
HO	0.54096-5	0.54292-5	0.18774-5	0.60852-6	0.58780-12	
O	0.0	0.10076-8	0.22344-9	0.23416-10	0.59079-12	
O_2	0.0	0.14816-9	0.67686-10	0.35557-11	0.63855-10	
H_2	0.74829	0.74784	0.74895	0.74797	0.74896	
H_2O	0.25029	0.25197	0.25031	0.25199	0.25031	
Pressure	2.675		1.483		0.000289	MN/m²
Temperature	1943.7		1707.4	1706.8	181.8	°K

Mixture Ratio = 5

Species	Chamber		Throat		Exit	
	Kinetic	Equil.	Kinetic	Equil.	Kinetic	Equil.
H	0.39112-1	0.38992-1	0.30324-1	0.30093-1	0.11704-1	0.24033-12
HO	0.25466-1	0.25674-1	0.17546-1	0.17632-1	0.15161-5	0.32559-16
O	0.16836-2	0.17036-2	0.91265-3	0.91602-3	0.10263-5	0.41084-28
O_2	0.10830-2	0.11089-2	0.60503-3	0.61382-3	0.15445-4	0.52322-28
H_2	0.35724	0.35426	0.35953	0.35652	0.36530	0.37
H_2O	0.57393	0.57826	0.58958	0.59423	0.62144	0.63
Pressure	2.682		1.545		0.000552	MN/m²
Temperature	3270.4		3073.7	3074.9	673.0	702.7 °K

Note: 0.12345-6 indicates 0.12345×10^{-6}

49

TABLE 8. CONCLUDED

Mixture Ratio = 8

Specie	Chamber		Throat		Exit	
	Kinetic	Equil.	Kinetic	Equil.	Kinetic	Equil.
H	0.40150-1	0.39827-1	0.35055-1	0.34684-1	0.36848-1	0.91922-5
HO	0.99538-1	0.10036	0.88605-1	0.89552-1	0.42106-2	0.46858-3
O	0.18700-1	0.19011-1	0.15892-1	0.16150-1	0.37820-2	0.58289-5
O_2	0.39588-1	0.40929-1	0.37959-1	0.39326-1	0.34466-1	0.41855-2
H_2	0.12643	0.12417	0.11753	0.11518	0.55165-1	0.64191-3
H_2O	0.67358	0.67570	0.70272	0.70511	0.85335	0.99469
Pressure	2.683		1.565		0.000797	MN/m^2
Temperature	3495.3		3339.1	3339.5	1154.0	1552.3 °K

Mixture Ratio = 12

Specie	Chamber		Throat		Exit	
	Kinetic	Equil.	Kinetic	Equil.	Kinetic	Equil.
H	0.15905.1	0.15804-1	0.12615-1	0.12475-1	0.16521-1	0.24038-10
HO	0.10918	0.10945	0.95251-1	0.95370-1	0.23449-2	0.44276-5
O	0.26276-1	0.26507-1	0.21833-1	0.21955-1	0.50322-2	0.76875-8
O_2	0.16392	0.17200	0.17300	0.17623	0.20287	0.20382
H_2	0.39602-1	0.39043-1	0.33523-1	0.32949-1	0.12416-1	0.16208-7
H_2O	0.63759	0.63719	0.66122	0.66102	0.75810	0.79518
Pressure	2.683		1.560		0.000721	MN/m^2
Temperature	3349.3		3186.0	3186.4	961.5	1078.3 °K

activation of the reactants, the high pressure will keep them closely packed, and the excess of one reactant means that the probability of completely reacting the other reactant becomes very high. In other words, the reactions are fast, and one reactant is depleted in the chamber. Therefore, all factors in the chamber conspire to produce a near-equilibrium concentration. This is also predicted by the TDK and ACE calculations.

For the case where the mixture ratio is such that stoichiometric ratios of oxidizer and fuel are present (mixture ratio = 8 for O/H), the situation is somewhat different. At equilibrium in the chamber, high temperature will cause some O and H species to be present, even at high pressure, since there is no available excess of either H or O to consume them. This again is shown by the TDK/ACE predictions for the chamber and throat at a mixture ratio of 8. After the throat, rapid expansion freezes the O and H species and prevents reaction to form H_2O. Therefore, the rate of reaction will determine how much H_2O is produced. The difference between the kinetic and equilibrium chemistry composition can be seen by comparing the composition at the exit plane for a mixture ratio of 8. There is still a relatively large amount of O, H and OH available to form H_2O, which would occur if the expansion had not caused the reaction rates to be dominant. The stoichiometric mixture ratio will probably have significant kinetic effects for other propellants as well. The magnitude of the kinetic effect on gas composition is shown in Figure 19 where the equilibrium and kinetic concentrations of water at the exit plane are plotted as a function of mixture ratio. It is very unlikely that liquid rocket motors would run a stoichiometric mixture ratio along the walls. This is probably the most severe kinetic case.

The effects of kinetics on the transport properties at the edge can be estimated by determining the properties at equilibrium and at kinetic compositions. The equilibrium expansion and kinetic expansion transport properties and heat capacities are compared in Table 9 at the exit plane. The largest effects are on the stoichiometric mixture ratio viscosity and conductivity, which show differences of 23 percent and 19 percent, respectively. This coupled with the results of Section 2.3.2 show that kinetic effects on the transport properties could have as much as a 10 percent difference in thrust loss at the exit and a 9 percent difference in heat flux to the wall for the most severe kinetic situations.

51
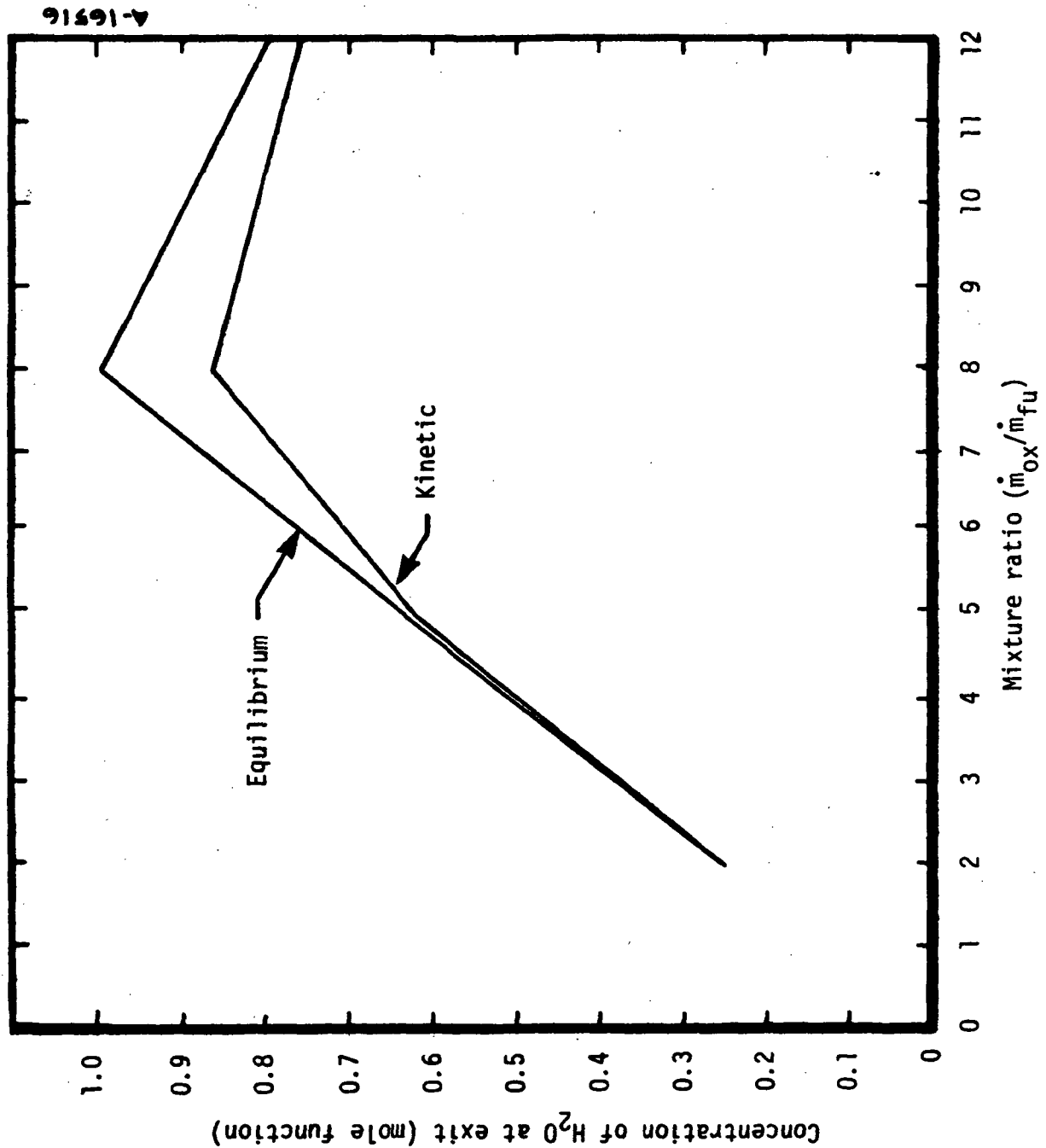
Figure 19. Variation of H_2O concentration as a function of mixture ratio of H/O system — kinetic and equilibrium.

TABLE 9. EQUILIBRIUM AND KINETIC COMPOSITION TRANSPORT
PROPERTIES AT THE EXIT PLANE (RL-10)

	MR = 5		MR = 8		MR = 12		
	Kinetic	Equil.	Kinetic	Equil.	Kinetic	Equil.	
Viscosity	0.24058-4	0.24788-4	0.36003-4	0.44187	0.32516-4	0.34185-4	$\frac{Nsec}{m^2}$
Conductivity	0.13427	0.13743	0.13715	0.16267	0.09538	0.10155	$\frac{watt}{m°K}$
Molecular weight	11.963	12.096	16.975	18.064	20.367	20.866	$\frac{kg}{kg-mole}$
Cp-equilibrium	2.886	2.894	2.440	2.737	1.938	1.971	$\frac{kJ}{kg°K}$
Cp-frozen	2.886	2.894	2.440	2.589	1.938	1.970	$\frac{kJ}{kg°K}$
Gamma	1.3171	1.3114	1.2511	1.2057	1.2668	1.2937	-----

In the interior of the boundary layer it is more difficult to make a
definite conclusion. A normal measure of the importance of chemical reaction
kinetics is the DamKöhler number (Da), which relates a characteristic reac-
tion time to a characteristic diffusion time. The reaction time is the reac-
tion rate of the slowest (or rate-controlling) reaction in the flow. The
diffusion time is the time for species to diffuse through the boundary layer.
If the ratio of diffusion to reaction times (Da = diffusion time/reaction
time) is large, then the reactions will be completed before the species can
move away; the flow will be in chemical equilibrium. If, however, the
DamKöhler number is small, then species will be diffusing faster than react-
ing, and it is expected that chemical kinetics would be important. Using the
flow conditions from a boundary layer solution in equilibrium at mixture ratio
around 5, and the pressure, temperature, and density from a kinetic expansion
(ODK) for mixture ratios of 5, 8, and 12 provides Damköhler numbers of 1000
at the throat and 1 at the exit. This indicates that kinetics are probably
not important in the boundary layer at the throat (as we've seen they're not
important for the throat edge conditions). However, near the exit plane,
kinetics could be important in the boundary layer provided there are suffi-
cient unreacted species.

The energetics of the boundary layer provide some more conclusions.
From the equilibrium and kinetic expansions, it was immediately clear that
the temperature of the flow was very sensitive to the enthalpy and composition.
For equilibrium compositions at the same enthalpies as the kinetic expansion,
the temperature of the stoichiometric edge went up by 52 percent from 1154°K
to 1753°K. This indicates that a considerable amount of energy can be car-
ried into the boundary layer by the diffusion of unreacted species. If the
reactions then take place in the boundary layer, the resultant heat release
could significantly alter the heat flux to the wall. In the off-stoichiometric
conditions, the temperature differences are much smaller (~10 percent) and this
effect would have much less impact.

In summary, for fuel-rich mixture ratios, there will probably not be
any significant kinetic effects in either the edge conditions or the boundary
layer up to the throat. From the throat on, there will probably not be any

kinetic effect on the edge conditions, although it is possible that the boundary layer is very slightly affected. For oxidizer-rich cases the same conclusions hold, although the effects may be more pronounced. For stoichiometric mixture ratios, kinetic effects will occur at the edge. The boundary layer will also be affected; although the impact of this on the heat flux and thrust loss could not be calculated.

Page
Intentionally
Left Blank

SECTION 5

PROCEDURES AND CODING

This section describes the suggestions for improvements for JANNAF compatibility and miscellaneous code modification. The objective of these tasks was to provide direction to the further development of BLIMP-J, and to correct or improve the capabilities of the code.

5.1 JANNAF COMPATIBILITY

This task defines the computational procedures which produce greater accuracy in the JANNAF methodology for predicting boundary layer effects. The first procedure shows how a circumferential variation in the flow properties could be handled, while the second provides for the effects of axial variation in mixture ratio. Both of these situations can occur in real liquid rocket engines due to imperfections in the injector flow pattern.

5.1.1 Nonaxisymmetric Streamtubes

The procedures discussed in this section demonstrate how BLIMP-J, formulated for axisymmetric flow, may be used to predict boundary layer effects for nonaxisymmetric flow conditions. This use of BLIMP-J is an approximation whose accuracy depends on the severity of the nonaxisymmetric behavior. The following procedures can be used to apply BLIMP-J results to nonaxisymmetric flows.

The quantities of interest are the boundary layer contribution to the thrust loss (ΔF) and the total heat transfer rate to the nozzle walls ($\dot{Q}$). These may be calculated from the following expressions:

PRECEDING PAGE BLANK NOT FILM

$$\Delta F = \int_0^{2\pi} \frac{\Delta F_B(\theta)}{2\pi} \, d\theta \qquad (9)$$

$$\dot{Q} = \int_0^{2\pi} \frac{\dot{Q}_B(\theta)}{2\pi} \, d\theta \qquad (10)$$

The terms $\Delta F_b(\theta)$ and $\dot{Q}_b(\theta)$ are the results of a series of BLIMP solutions. Each solution is for a "locally" axisymmetric region. The output of BLIMP-J is in terms of a circular cross section; therefore, division by 2π is required to obtain the "per radian" values of $\Delta F_B(\theta)$ and $\dot{Q}_B(\theta)$ at the exit plane.

The number of BLIMP solutions required depends upon the asymmetry of the flow and the behavior with respect to θ of the functions $\Delta F_B(\theta)$ and $\dot{Q}_B(\theta)$. The nonaxisymmetric results for ΔF and $\dot{Q}$ can then be obtained from Equations (9) and (10) by an appropriate numerical integration technique.

5.1.2 Axial Variation in Mixture Ratio

Some cases may require consideration of axial variations in the mixture ratio of the propellant. For example, if the injector pattern creates significant radial striations in the flow, a multiple zone TDK solution may be used to predict the inviscid flow. In this case, both the mixture ratio and total enthalpy may change from zone to zone. If the mass in the boundary layer exceeds the mass in the first zone (wall zone), then the second zone flow properties (total enthalpy, mixture ratio, pressure, and velocity) can be used as edge conditions for the boundary layer. The BLIMP-J program is not presently coded to allow such changes, but modifications could be made. However, numerical convergence problems may arise if the changes between zones are too extreme or if the BLIMP solution stations between which the changes occur are too close together.

A computational procedure and the appropriate code modifications which account for the axial variations in mixture ratio and total enthalpy are discussed below. It is possible (and preferable) to automate the procedure which, as described here, is assumed to be external to the operation of the code. An external procedure does, however, allow some discretion in how the transition

between zones is made. For example, if the changes are severe, it may be prudent to "smear" them out over two or three stations.

The computational procedure which can be used to solve a multiple zone boundary layer problem is outlined below:

- Input to BLIMP the zone one values for mixture ratio, total enthalpy, pressure, and velocity. Run BLIMP. If the mass in the boundary layer does not exceed the mass in the wall zone (M_1), no further effort is required.

- If the mass in the boundary layer does exceed M_1, modify the BLIMP input so that the zone two inviscid flow properties are used for all input downstream of (and including) the station at which the boundary layer mass exceeded M_1. This station will be referred to as the "stop." (The user may choose to spread the changes between zones over several stations.) A minor code modification is required to account for the change in total enthalpy between zones.

- Restart BLIMP upstream of the "stop" or rerun the entire problem. The station upstream of the "stop" should be identified as a discontinuity.

This procedure may be repeated as often as necessary to complete the solution; however, it would be unusual for the boundary layer to extend beyond the second zone.

Modifications to BLIMP-J which would be required if the above procedure was built-in to the code are described below. The actual code changes have not been written.

- Add to the code new variables and new input
    - Axial variation in mixture ratio
    - Axial variation in total enthalpy
    - Elemental composition of oxidizer
    - Elemental composition of fuel
    - Enthalpy of oxidizer and fuel prior to injection
    - Total mass flux allowed in the boundary layer

59

- Modify the main chemistry subroutine (EQUIL, B20A) to account for changes in mixture ratio and total enthalpy. This will allow new values of the edge concentration to be calculated and stored for each change in mixture ratio

- Modify the main subroutine of the boundary layer iteration procedure so that the NETA node (edge) values for total enthalpy and base species concentrations are set to the appropriate inviscid edge value prior to the beginning of each boundary layer solution

- Modify the output subroutine (OUTPUT, B11A) to cause the program to stop if the mass in the boundary layer exceeds total mass in zone one

This procedure and the code modifications have not been tested. They are intended to illustrate a possible method for treating axial variations in the mixture ratio.

5.2 MISCELLANEOUS CODE MODIFICATIONS

The object of this task was to generate and document FORTRAN changes to the BLIMP-J code to account for (1) the JANNAF method of computing thrust loss with mass addition from the walls and (2) simplified input of chamber conditions. The FORTRAN changes are referenced to the listing of the code as given in the BLIMP-J User's Manual (Reference 8). The subroutine name is given and the changes noted as if being directly input to the UNIVAC 1108 FORTRAN compilers: the changes between cards M and N (inclusive) are signaled by -M, N preceding the changed cards. The statement "-M" signifies that the cards following are to be inserted immediately after card number M.

5.2.1 Thrust Loss Calculation

This modification takes in account the different thrust lost by the boundary layer for TDK and BLIMP due to mass addition from the walls. Three cards are added after Card 304 of B11A:

```
"FOR.US   B11A
-304
C                                             TO ACCOUNT FOR JANNAF THRUST LOSS
      DF=DF + 2.*RADFL(6)*SQRT(2.*XI(IS))*F(1,1)*UE(IS)
     $   *GF(IS+10)/32.174/HCL**2/UCS
```

5.2.2 Simplified Chamber Conditions

This modification allows the user to input the enthalpies of fuel and oxidizer and the mixture ratio (ratio of oxidizer mass flowrate to fuel mass flowrate). From this data the chamber enthalpy is computed from the following formula:

$$h_0 = \frac{MR * h_{ox} + h_{fu}}{MR + 1}$$

To utilize this option, the fuel and oxidizer specific (mass) enthalpies in J/kg (or Btu/lbm) and the mixture ratio (MR) are necessary. The enthalpy per unit mass of oxidizer and fuel can be obtained from the molar enthalpies by dividing by the molecular weights of the oxidizer and fuel, respectively. For the NAMELIST input format, the variable KEY of NAMELIST $INPUT must be nonzero to activate this option. The variables RMX, HOX, and HFU should contain the mixture ratio, the enthalpy of the oxidizer, and the enthalpy of the fuel, respectively.

The FORTRAN changes are:

```
"FOR,US   B09A
-274,274
      READ(KIN,1820) GE(1),KEY,HFU,RMX
 1820 FORMAT(E10.4,I1,2E10.4)
      IF(KEY.EQ.0) GO TO 1821
      HOX=GE(1)
      GE(1)=(RMX*HOX+HFU)/(RMX+1.)
 1821 CONTINUE
-283
      IF(KEY.NE.0) WRITE(KOUT,1822) RMX,HOX,HFU
 1822 FORMAT(15X,14HMIXTURE RATIO=,F10.3/15X,18HOXIDIZER ENTHALPY=,
     $    1PE12.5/15X,14HFUEL ENTHALPY=,1PE12.5)
"FOR,US   B07B   .
-27
      4,KEY,RMX,HOX,HFU
-31
      KEY=0
-83
      IF(KEY.NE.0) GE(1)=(RMX*HOX+HFU)/(RMX+1.)
```

5.2.3 Other Changes

The following FORTRAN changes are minor corrections to the code. They have no effect on the sample cases or on most cases that would be run. All corrections are referenced to the line numbers in the code listing of Section 4 of Reference 8.

```
"FOR,US   B07A
-54,54
   33 FORMAT(/,1X,17HFLUX NORM. PARAM,A6,PE12.5/(24X,PE12.5))
-194
      IF(M.EQ.NS) GO TO 111
-289
C***   THE VARIABLES SLUM1.....FWCON ARE USED FELOW FOR TEMP. STORAGE.
-292,292
      C3M(I)=PE(I,1)/UCP
-305,305
      WRITE(KOUT,25)KA(N,2),(C3M(I),I=1,NS)
-315
    1 C3M,FWDUM,BETAM,BETAV
-317
      V=UCN/UCL/UCL
-324,324
  178 XICON(I)=-1.0/C3M(I)/V
      WRITE(KOUT,33)KA(N,12),(XICON(I),I=1,NS)
-333
      IF(NL.NE.0) GO TO 107
-370,370
 1173 RHOVW(J,1)=RHOVW(J,1)*V*C3M(J)
-403
      IF(MM.EQ.NS)GO TO 604
-409,410
"FOR,US   B07E
-78,80
      ELCON= .4
      YAP= -11.8
      CLNUM= .0158
"FOR,US   B14A
-9,9
    3,KAUXO,JTTRE,JSPEC,NU(3),IU
-114,114
      IF(IU+ITEM-2)301,301,302
"FOR,US   B14C
-5,6
      HHOMO  =A(6,L)+T*(A(1,L)+T*(A(2,L)/2.+T*(A(3,L)/3.+T*(A(4,L)/4.+T*
     1A(5,L)/5.))))
```

```
"FOR.US  B204
-68,68
      TTMAX=12000.

-411
      L=IUNIT+1
"FOR.US  650F
-15,16
-46,48
  202 A(N)=(PP(N+1)+PP(N)-2.*(P(N+1)-P(N))/DETA(N))/DETA(N)/DETA(N)
      B(N)=(PP(N+1)-PP(N)-3.*A(N)*(ETA(N+1)*ETA(N+1)-ETA(N)*ETA(N)))/2.
      1 /DETA(N)
      C(N)=PP(N+1)+ETA(N+1)*(PP(N)-PP(N+1))/DETA(N)+3.*A(N)*ETA(N)*
      1 ETA(N+1)
```

Page Intentionally Left Blank

SECTION 6

CONCLUSIONS AND RECOMMENDATIONS

Conclusions

1. There is insufficient experimental data available to fully determine which turbulence model is most applicable to SSME operating conditions.

2. The Cebeci-Smith turbulence model provides the best overall agreement with the available data and is therefore recommended as the standard turbulence model.

3. Uncertainties in the mixture ratio of the propellant gases near the wall may cause more error in the boundary layer calculations than inaccuracies in the turbulence model do.

4. The boundary layer test program described in Section 3 would yield data sufficiently accurate to verify which model is most accurate.

5. The unequal diffusion coefficient without thermal diffusion option and with built-in diffusion factors should be the normal running mode, unless computation time is constrained.

6. The turbulent boundary layer predictions are insensitive to moderate variations in the transport properties, and the ideal gas law is adequate for the flow conditions in the SSME.

7. The REFIT option is extremely valuable in determining optimum nodal positions and providing improved accuracy for most calculations. When extreme accuracy is necessary, it should not be used for the final results.

8. For hydrogen/oxygen systems and flow conditions appropriate to the SSME and RL-10 engines, chemical reaction kinetics are probably unimportant, except at stochiometric conditions.

65

9. The BLIMP code can be modified to consider axial variation in the mixture ratio.

Recommendations

1. The capability to determine the mixture ratio of the gases in the region near the wall should be assessed. Accurate prediction of this mixture ratio is essential since it has a significant impact on the boundary layer predictions.

2. The procedure for axial variation of the mixture ratio as defined in Section 5.1.2 should be implemented.

3. An additional oxidizer/fuel combination should be investigated for homogeneous gas phase kinetic effects. If kinetics are shown to be important at a later time, then a kinetics package for BLIMP-J should be defined.

4. Versions of BLIMP-J should be prepared and checked out for use on CDC and IBM machines. This will assist the user community to easily implement BLIMP-J on the other systems.

REFERENCES

1. Evans, R. M., "JANNAF Boundary Layer Integral Matrix Procedure," Aerotherm Final Report 75-152, July 1975.

2. Back, L. H. and Cuffel, R. F., "Turbulent Boundary Layer and Heat Transfer Measurements Along a Convergent-Divergent Nozzle," Journal of Heat Transfer, pp. 397-407, November 1971.

3. Nerem, R. M. and Hopkins, R. A., "An Experimental Investigation of Heat Transfer from a Highly Cooled Turbulent Boundary Layer," AIAA Paper 68-43, New York, New York, January 22-24, 1968.

4. Hopkins, R. A., "Measurements of Turbulent Heat Transfer Rates to a Highly Cooled Surface with Zero Pressure Gradient in Partially Dissociated Air," M.S. Thesis, Ohio State University, Department Aero. & Astro. Engr., 1967.

5. Jones, J. J., "Shock-Tube Heat-Transfer Measurements on Inner Surface of a Cylinder (Simulating a Flat Plate) for Stagnation-Temperature Range 4100°R - 8300°R," NASA TN D-54, September 1959.

6. Bird, R. B., et al., Transport Phenomena, pp. 17, 252, and 506, John Wiley and Sons, Incorporated, New York, New York, 1960.

7. Lee, J. F. and Sears, F. W., Thermodynamics, p. 55, Addison-Wesley, Palo Alto, California, 1963.

8. Evans, R. Michael, "Boundary Layer Integral Matrix Procedure, BLIMP-J User's Manual," Aerotherm UM-75-64, July 1975.

9. Romine, W. D., Internal letter, Rockwell International Corp., PAM 3112-2040-ASR 74-98, SSME 74-1014, 10 October 1973.

Page
Intentionally
Left Blank

APPENDIX A

LIST OF SYMBOLS

A_j, b_j Van der Wall gas constants for chemical species j

C_p Specific heat at constant pressure

D Diffusivity

G Gibbs free energy (chemical potential)

g_c 32.174 lb_m-ft/lb_f-sec^2 for English units; 1 for SI units

H Enthalpy

k Thermal conductivity

MR Mixture ratio (flowrate of oxidizer/flowrate of fuel)

P Pressure (absolute)

Pr Prandtl number

$\dot{Q}$ Total heat flux

$\dot{q}$ Heat flux

R Gas constant

Re' Unit Reynolds number $(\rho_e u_e / \mu_e)$

Re_θ Reynolds number based on momentum thickness

Re_x Reynolds number based on running length

S Entropy

St	Stanton number
T	Temperature
U_s	Shock velocity in shocktube experiments
u	Velocity
v,V	Specific volume
y_i	Mole fraction of gaseous species
Z	Compressibility ($P/\rho RT$)
γ	Ratio of heat capacities (C_p/C_v)
ΔF	Thrust loss
δ	Boundary layer thickness
ϵ	Eddy viscosity
ϵ	Expansion ratio (local area/throat area)
ρ	Density
τ_w	Wall shear stress
μ	Viscosity

Subscripts

o	Stagnation (chamber) condition
w	Wall condition
e	Edge of boundary layer
c	Critical condition
r	Reduced property (property value at local conditions/property value at critical conditions)

APPENDIX B

PROCEDURE FOR USE OF REFIT OPTION

For the most effective use of the REFIT option the following procedures are recommended:

- Use REFIT with the built-in nodal distribution and REFIT parameters for the preliminary cases, and whenever the very slight inaccuracies resulting from its use are acceptable (slight modification to the built-in parameters may be necessary for some problems).

- Use the results of the REFIT case to select a nodal distribution adequate for the entire length of the body. For turbulent flows, this will usually require more than 12 nodes.

- Compare the results of the cases described above to assess the impact of REFIT for the particular problem.

A graphical procedure for selection of the nodes between $u/u_e = 0$ and 0.95 (the KAPPA node) is shown in Figure B-1. The velocity at the first and last solution stations are plotted on a semilog scale. (It is sometimes useful to include an intermediate station.) The nodes between η_2 and η_{KAPPA} ($u/u_e = 0.95$) are selected so that the velocity values between $u/u_e = 0.05$ and 0.95 are approximately evenly distributed for both profiles. The resulting nodal distribution is shown in Figure B-1.

For both profiles, the nodal distribution is well spaced throughout the velocity range. It is typical that the well developed profile at the last station requires a few nodes much closer to the wall than that required by the profile at the first station. It should be noted that the η's are approximately evenly spaced in log (η), resulting from the linear nature of u/u_e with respect to log (η).
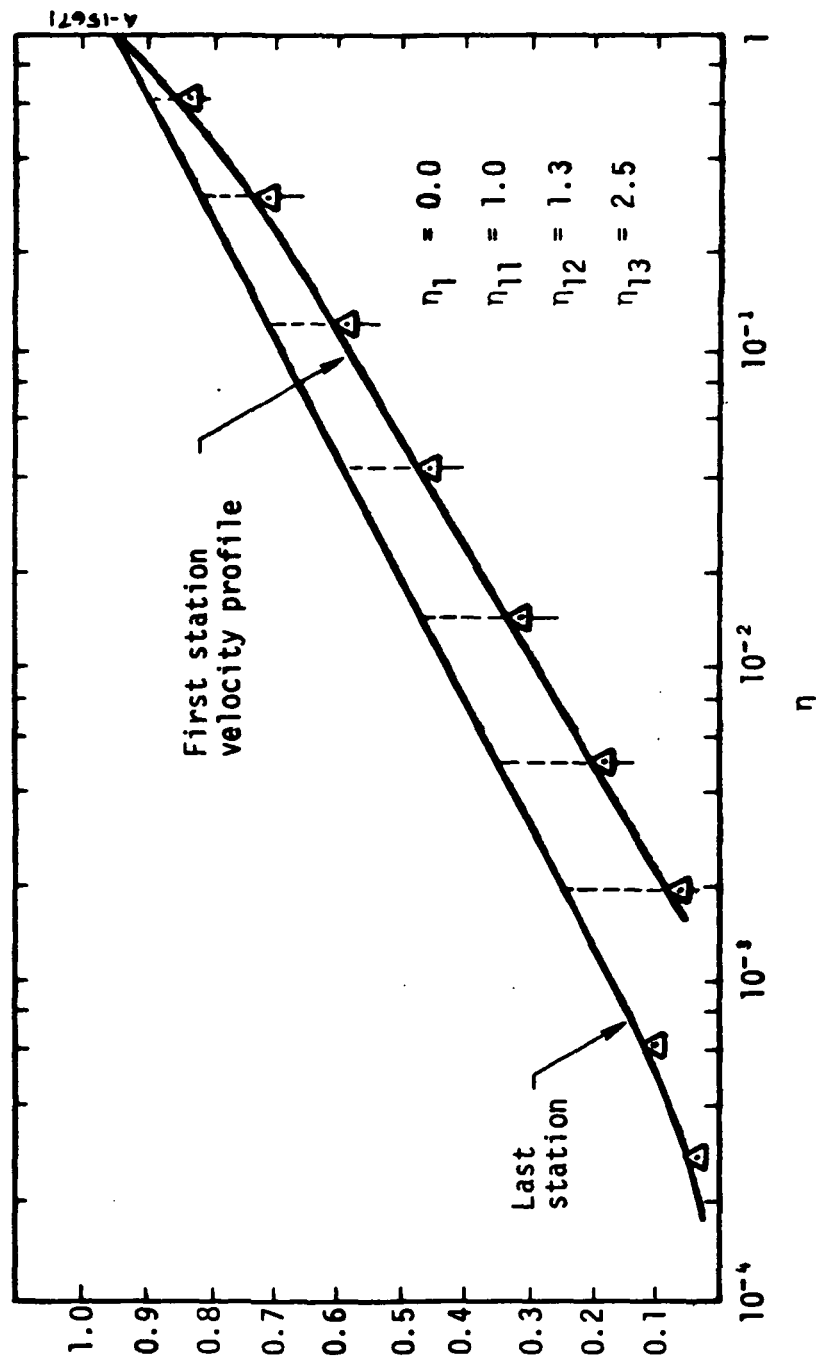
Figure B-1. Selection of nodes for "NO REFIT" case (velocity profiles taken from SSME "REFIT" case).

Selection of the nodes by the method described above generally re-
sults in a set of η's applicable to the entire nozzle. However, all velocity
profiles should be checked to ensure that this is, in fact, the case.